

1 **Constraints on Southern Ocean Shortwave Cloud**
2 **Feedback from the Hydrological Cycle**

3 **Chuyan Tan^{1*}, Daniel T. McCoy¹, Gregory S. Elsaesser^{2,3}**

4 ¹University of Wyoming, Laramie, WY, USA

5 ²Columbia University, Dept. of Appl. Physics and Appl. Mathematics, New York, NY, USA

6 ³NASA Goddard Institute for Space Studies (GISS), New York, NY, USA

7 *Now at: Hunan Climate Center, Changsha, China

8 **Key Points:**

- 9 • Southern Ocean liquid water path increased over the past two decades due to en-
10 hanced moisture convergence.
11 • Enhanced moisture convergence contributes to a negative cloud feedback in the
12 Southern Ocean.
13 • Across global climate models, the sensitivity of upwelling shortwave to cloud op-
14 poses the sensitivity of cloud to moisture convergence.

Abstract

Shifts in Southern Ocean (SO, 40 – 85°S) shortwave cloud feedback (SW_{FB}) toward more positive values are the dominant contributor to higher effective climate sensitivity (ECS) in Coupled Model Intercomparison Project phase 6 (CMIP6) models. To provide an observational constraint on the SO SW_{FB} , we use a simplified physical model to connect SO SW_{FB} with the response of column-integrated liquid water mass (LWP) to warming and the susceptibility of albedo to LWP in 50 CMIP5 and CMIP6 GCMs. In turn, we predict the responses of SO LWP using a cloud-controlling factor (CCF) model. The combination of the CCF model and radiative susceptibility explains about 50% of the variance in the GCM-simulated SW_{FB} in the SO. Observations of SW radiation fluxes, LWP, and CCFs from reanalysis are used to constrain the SO SW_{FB} . The response of SO LWP to warming is constrained to $2.76 - 4.19 \text{ g m}^{-2} \text{ K}^{-1}$, relative to a GCM prior of $0.64 - 9.33 \text{ g m}^{-2} \text{ K}^{-1}$. The susceptibility of albedo to LWP is constrained to be $0.43 - 0.90 (\text{kg m}^{-2})^{-1}$, relative to $0.30 - 3.91 (\text{kg m}^{-2})^{-1}$. The overall constraint on the contribution of SO to global mean SW_{FB} is $-0.168 - 0.051 \text{ W m}^{-2} \text{ K}^{-1}$, relative to $-0.277 - 0.270 \text{ W m}^{-2} \text{ K}^{-1}$. In summary, observations suggest SO SW_{FB} is less likely to be as extremely positive as predicted by some CMIP6 GCMs, but more likely to range from moderate negative to weakly positive.

Plain Language Summary

Previous studies suggest that SO clouds reflect more sunlight in response to global warming and more strongly cool the planet - a negative shortwave cloud feedback (SW_{FB}). The SO SW_{FB} in the latest generation of global climate models (GCMs) participating in the Coupled Model Intercomparison Project phase 6 (CMIP6) has shifted toward more positive values, leading to the larger predicted temperature responses to greenhouse gas increases in these GCMs. In this study, we examine if this more positive SW_{FB} is consistent with observations. We connect the effect of SO clouds on reflected sunlight with the predicted response of cloud liquid content to global warming. The linkage between cloud liquid water content and large-scale meteorology is applied to predict this cloud liquid response. Satellite observations of reflected sunlight, cloud liquid, and observations of large-scale meteorology are applied to constrain the SO SW_{FB} for 50 CMIP5 and CMIP6 GCMs. The results suggest that SO cloud liquid will increase with warming around the average of predictions of 50 GCMs. Satellite records suggest that the sensitivity of reflected sunlight to cloud liquid is weak compared to GCMs. In combination, our results suggest SO clouds most likely reflect more sunlight back to space and further cool our planet.

1 Introduction

Quantifying the surface temperature response to a doubling in atmospheric CO_2 concentration, commonly referred to as climate sensitivity, is a fundamental goal of climate science (Houghton & el., 2001; Boucher & el., 2014; Forster & el., 2023). Climate feedback processes such as changes in lapse rate, water vapor, and cloud may dampen or amplify the temperature response to greenhouse gas increase and are critical for estimating climate sensitivity (Bony et al., 2006). Global climate models (GCMs) provide the most direct way to estimate climate sensitivity since they attempt to simulate all relevant processes, including climate feedback (Andrews et al., 2012; Zelinka, Myers, McCoy, Po-Chedley, et al., 2020). Shortwave cloud feedback (SW_{FB}), the shortwave (SW) radiative impact of cloud responses to a surface temperature perturbation, is the largest uncertainty in GCMs' estimate of net climate feedback and by extension, climate sensitivity (Zelinka, Myers, McCoy, Po-Chedley, et al., 2020; Sherwood et al., 2020). The uncertainty in estimating SW_{FB} is strongly driven by difficulties in representing subgrid-

64 scale cloud processes in GCMs (Storelvmo et al., 2015; Webb et al., 2015; Sherwood et
65 al., 2014; Zhao, 2014).

66 Despite the large intermodel spread in global-mean SW_{FB} , robust regional features
67 have emerged from previous generations of GCMs. For example, positive SW_{FB} in the
68 subtropics has emerged, likely due to decreased cloud coverage with negative SW_{FB} in
69 the middle-to-high latitudes likely attributed to increased cloud optical depth (Zelinka
70 et al., 2012; Ceppi, McCoy, & Hartmann, 2016). Considerable progress has been made
71 on narrowing the possible ranges of tropical and subtropical SW_{FB} using observational
72 constraints (Myers et al., 2021; G. V. Cesana & Del Genio, 2021; G. Cesana et al., 2019;
73 Scott et al., 2020; Klein et al., 2017).

74 Recent GCMs have suggested a weaker negative Southern Ocean (SO, $40-85^{\circ}S$)
75 SW_{FB} . The ensemble mean SO SW_{FB} of GCMs participating in the sixth phase of the
76 Coupled Model Intercomparison Project (CMIP6) has shifted toward a more positive value
77 relative to CMIP5, leading to the emergence of several GCMs with high effective climate
78 sensitivity (ECS) ($ECS \geq 4.5K$) (Zelinka, Myers, McCoy, Po-Chedley, et al., 2020; Bodas-
79 Salcedo et al., 2019). Much effort has been made to understand this change within the
80 context of GCM cloud physics (Bjordal et al., 2020; Bodas-Salcedo et al., 2019; Gettel-
81 man et al., 2019; Zhang et al., 2019). The uncertainty in ECS owing to SO SW_{FB} is still
82 largely unconstrained by observations (Sherwood et al., 2020), with only a few studies
83 explicitly focusing on evaluating SO SW_{FB} using the observational records of clouds,
84 radiation, and meteorology (Terai et al., 2019, 2016; Ceppi, McCoy, & Hartmann, 2016;
85 Gordon & Klein, 2014; Tan et al., 2019; Norris et al., 2016).

86 Many mechanisms have been proposed to explain the origins of negative SO SW_{FB}
87 (Terai et al., 2019; Sherwood et al., 2020). One potential explanation is increasing liq-
88 uid water content (LWC) from the warmer moist adiabat (Betts & Harshvardhan, 1987;
89 Terai et al., 2019; Frazer & Ming, 2022). Shifts in the moist adiabat as the atmosphere
90 warms will increase cloud LWC if the geometric height of clouds is preserved. As cloud
91 temperature increases, the change in LWC per degree of warming decreases rapidly, so
92 this mechanism is only salient in the high latitudes (Terai et al., 2019). Another poten-
93 tial mechanism is the increase in cloud LWC driven by shifts in the cloud phase (Senior
94 & Mitchell, 1993; Tan et al., 2019, 2016; McCoy et al., 2014). As the atmospheric tem-
95 perature rises, cloud condensates shifts from ice to liquid in the mixed-phased cloud re-
96 gions. The total water content may also increase because liquid precipitates less efficiently
97 than ice (Ceppi, Hartmann, & Webb, 2016; Frazer & Ming, 2022). In recent literature,
98 a mechanism based on the connection between hydrological response and cloudiness change
99 has been proposed to explain the increased LWC in extratropics (McCoy et al., 2022;
100 McCoy, Field, Bodas-Salcedo, et al., 2020; McCoy et al., 2019). All aforementioned mech-
101 anisms may contribute to an increase in in-cloud LWC, which results in a negative cloud
102 optical depth feedback (Stephens, 1978). Other mechanisms may contribute to changes
103 in cloud coverage in the SO. These processes are restricted to boundary layer (BL) clouds.
104 When the capping inversion at the top of BL increases with warming, the cloud top en-
105 trainment will be suppressed and lead to an increase in BL cloudiness (Bretherton et al.,
106 2013; Myers & Norris, 2013; Qu et al., 2015). However, the cloud top entrainment may
107 also increase with warming because of the increased vertical humidity gradient between
108 BL and free troposphere (Bretherton et al., 2013; Frey & Kay, 2018; Rieck et al., 2012).
109 This will reduce the BL cloudiness. The decoupling in the BL may increase with warm-
110 ing, preventing moisture transports from the surface into the cloud layer and also de-
111 creasing the low-cloud amount (Bretherton & Wyant, 1997; Bretherton et al., 2013; Zheng
112 et al., 2020). All these hypothesized mechanisms may contribute to SO SW_{FB} and are
113 entangled with each other, making process-level constraint of the SO SW_{FB} difficult (Terai
114 et al., 2019; Frazer & Ming, 2022).

115 Here, we seek to provide a constraint on the GCM ensemble SO SW_{FB} using ob-
116 served cloud properties and their covariability with meteorological state. The existing

117 research has examined various cloud properties such as shortwave cloud radiative effect
 118 (SWCRE), albedo, cloud optical depth, and cloud fraction to provide observational con-
 119 straints on the extratropical SW_{FB} (Gordon & Klein, 2014; Qu et al., 2015; Ceppi, Mc-
 120 Coy, & Hartmann, 2016; Norris et al., 2016; Terai et al., 2016; Myers et al., 2021; Mc-
 121 Coy et al., 2022). They generally support a positive SW_{FB} related to BL clouds and a
 122 negative SW_{FB} related to upper level clouds, and an overall negative extratropical SW_{FB} .
 123 Many of these studies have had to contend with the availability of GCM data and the
 124 challenges in characterizing SO clouds using visible radiation. GCM cloud fraction and
 125 cloud optical depth have to be processed with satellite simulators to enable direct com-
 126 parison between model output and satellite retrievals (Bodas-Salcedo et al., 2011). The
 127 number of models that provide these outputs is very restricted, which limits evaluation
 128 of the shift in SO SW_{FB} spanning a large number of GCMs across CMIP5 and CMIP6
 129 (Gordon & Klein, 2014; Ceppi, McCoy, & Hartmann, 2016). The SO also presents an
 130 observational challenge. Satellite retrievals of low-topped cloud properties like low-cloud
 131 fraction are difficult because of the multilayered structure of SO clouds (Qu et al., 2015;
 132 Haynes et al., 2011; Marchand et al., 2009; Sourdeval et al., 2016). Top-of-atmosphere
 133 (TOA) radiative flux derived quantities like SWCRE and albedo are more directly com-
 134 parable to GCM output (Loeb et al., 2020), but they combine the effects of radiative pro-
 135 cesses as well as the response of clouds to meteorology. This makes it difficult to unpick
 136 how variations in TOA radiation are related to large-scale meteorology (Myers et al., 2021).

137 Area-mean column-integrated liquid water mass (LWP) is an advantageous cloud
 138 property for constraining SO cloud variability because the comparison between CMIP
 139 GCM output and low-frequency microwave radiometers is relatively straightforward. The
 140 LWP reported by GCMs and microwave observations is averaged over cloudy and cloud-
 141 free scenes and variability in LWP combines variability in cloud coverage and in-cloud
 142 LWC. LWP is a standard model output for all CMIP5/6 GCMs and can be directly com-
 143 pared to microwave observations without a satellite simulator as long as attention is paid
 144 to separating precipitating and non-precipitating liquid. Microwave LWP retrieval is not
 145 sensitive to multi-layered clouds, making it optimal for constraining SO cloud variabil-
 146 ity without partitioning by cloud top pressure regimes and accounting for overlap (McCoy
 147 et al., 2014). The response of area-mean LWP to warming is anti-correlated with SW_{FB}
 148 in the SO (Stephens, 1978; McCoy et al., 2022). For the above reasons, we choose to con-
 149 strain the SO SW_{FB} across CMIP5 and CMIP6 models by constraining the response of
 150 LWP to warming.

151 We predict SO LWP response by the linkage between clouds and large-scale me-
 152 teorology (so-called cloud-controlling factor (CCF) analysis, Stevens and Brenguier (2009)).
 153 Observations of clouds and their environment can be used to infer the response of clouds
 154 to long-term warming by assuming the relationships between clouds and large-scale me-
 155 teorology are invariant from shorter observed periods (days - years) to climate change
 156 time-scale (years - century) (Klein et al., 2017). Surface temperature, stability, and large-
 157 scale subsidence have been widely used as environmental factors to predict cloud responses
 158 (Grise & Medeiros, 2016; Frey & Kay, 2018; McCoy, Field, Gordon, et al., 2020; McCoy,
 159 Field, Bodas-Salcedo, et al., 2020; Myers et al., 2021). In addition to these quantities,
 160 our CCF analysis considers large-scale moisture convergence. As shown in Held and So-
 161 den (2006), column-integrated water vapor increases with warming following Clausius-
 162 Clapeyron (C-C) scaling. Two direct consequences of increased humidity are increased
 163 horizontal transport of water vapor and enhanced existing patterns of moisture conver-
 164 gence and divergence. The latter change also satisfies the C-C scaling, albeit with spa-
 165 tial adjustments such as poleward expansion of the drying region (Siler et al., 2018; Bo-
 166 nan et al., 2023). Local precipitation and evaporation in the extratropics increase with
 167 warming but at a slower rate than C-C scaling owing to the energetic constraints (Allen
 168 & Ingram, 2002; Lorenz & DeWeaver, 2007; Stephens & Ellis, 2008; Trenberth, 2011; Yet-
 169 tella & Kay, 2017). The effects of a strengthening hydrological cycle in response to warm-
 170 ing is consistent with how SO LWP responds to warming (McCoy et al., 2019). Because

171 the conversion of water vapor to precipitation happens in clouds, increases in both the
 172 source and sink of clouds should guarantee an increase in cloudiness. In this work, we
 173 evaluate the linkage between the hydrological cycle and SO SW_{FB} by using moisture con-
 174 vergence as one of the large-scale meteorology factors to predict the SO LWP response
 175 (McCoy, Field, Bodas-Salcedo, et al., 2020; McCoy et al., 2022).

176 In addition to constraining the cloud response to meteorology, it is necessary to con-
 177 strain the interactions between clouds and the radiation to constrain SW_{FB} . Previous
 178 work has shown that GCMs differ substantially in their simulation of how increasing cloudi-
 179 ness affects TOA upwelling SW flux (Bender et al., 2017). The intermodel differences
 180 in the radiative susceptibility of TOA SW flux to LWP contribute strongly to the inter-
 181 model difference in the SO SW_{FB} (McCoy et al., 2022). Model biases in simulating cloudi-
 182 ness changes in a perturbed climate are likely being compensated by the biases in the
 183 optical properties of simulated clouds. The so-called 'Too few, Too bright' bias has been
 184 diagnosed in previous generations of GCMs in the tropics (Nam et al., 2012; Konsta et
 185 al., 2022).

186 The goal of this paper is to use observations to constrain the SO SW_{FB} across 50
 187 CMIP5 and CMIP6 GCMs (Table S1). A simplified physical model is developed to pre-
 188 dict GCM SW_{FB} calculated from radiative kernels (Zelinka, Myers, McCoy, Po-Chedley,
 189 et al., 2020) by using the responses of LWP to warming combined with the susceptibil-
 190 ity of radiation to liquid. Then, we constrain the LWP response to warming of GCMs
 191 by the observed covariability between LWP and large-scale meteorology, focusing on the
 192 role of hydrological response on SO SW_{FB} . Following this, we use satellite observations
 193 to calculate the susceptibility of radiation to liquid. Combining the constraints on LWP
 194 response and radiative susceptibility, we produce a constraint on the SO SW_{FB} . The
 195 paper is organized as follows. Section 2 describes the GCMs and observations, the sim-
 196 plified physical model, and how observations are used to constrain GCM SW_{FB} . In sec-
 197 tion 3, we conduct step-by-step constraints on the LWP response, radiative susceptibil-
 198 ity, and the SO SW_{FB} of GCMs. Section 4 presents conclusions of this study and sug-
 199 gestions for future work on constraining extratropical SW_{FB} .

200 2 Data and Methodology

201 2.1 Data

202 We use 50 GCMs participating in CMIP5 (20) and CMIP6 (30) to provide the prior
 203 distribution of SO SW_{FB} . GCMs and their SO ($40-85^{\circ}S$) SW_{FB} are listed in Table
 204 S1. The SW_{FB} for all GCMs are provided by Zelinka, Myers, McCoy, Po-Chedley, et al.
 205 (2020). For each GCM, Zelinka, Myers, McCoy, Po-Chedley, et al. (2020) calculate the
 206 response of SWCRE (clear-sky minus all-sky upwelling SW flux at TOA) to warming in
 207 the fully coupled 150-year CO_2 quadrupling (*abrupt4xCO₂*) simulation. SW_{FB} is ob-
 208 tained by adjusting the SWCRE response for non-cloud influences. This was completed
 209 by employing all- and clear-sky radiative kernels to discern the change in SWCRE due
 210 to clouds from other perturbations (e.g., water vapor, surface albedo, and external forc-
 211 ing) (Huang et al., 2017; Soden et al., 2008; Shell et al., 2008). The SW_{FB} output is spatially-
 212 resolved (1° gridded) the region $90^{\circ}S - 90^{\circ}N$.

213 We use monthly-mean LWP, global-mean near-surface temperature (GMT), large-
 214 scale meteorology, and TOA SW flux from fully-coupled preindustrial control (*piControl*)
 215 and *abrupt4xCO₂* GCM simulations to construct a simplified physical model linking vari-
 216 ability in LWP to SW_{FB} . Using monthly-mean output instead of higher temporal res-
 217 olution output allowed us to survey nearly all CMIP5 and CMIP6 GCMs. LWP is the
 218 column-integrated liquid water mass averaged over cloudy and cloud-free portions of the
 219 model gridbox, which can be related to in-cloud LWP and cloud fraction since $LWP \approx$
 220 cloud fraction \times in-cloud LWP. LWP is computed as the difference between CMIP vari-

ables *clwvi* (total condensed water path) and *clivi* (ice water path, IWP). We calculate the change in GMT (*tas*) in each GCM to normalize the change in LWP for consistency with the calculation of SW_{FB} (Zelinka, Myers, McCoy, Po-Chedley, et al., 2020). Four descriptors of large-scale meteorology are used to predict the SO LWP: surface skin temperature (T_s ; labeled *ts* in CMIP output); precipitation minus evaporation ($P-E$; *pr* and *hfls*), a proxy for moisture convergence; lower-tropospheric stability (*LTS*; calculated from *ta* at 700 mb, *ps*, and *ts*) (Klein & Hartmann, 1993), and subsidence at 500 mb (ω_{500} ; *wap*). Note that T_s refers to the skin temperature of Earth’s surface, which differs from the near-surface air temperature used to calculate GMT (output from CMIP as *tas*). For the open ocean, T_s is the sea surface temperature. GCM radiative susceptibility is calculated from the TOA albedo (α calculated from the CMIP outputs *rsut/rsdt*), LWP, and clear-sky albedo ($\alpha_{cs} = rsutcs/rsdt$) (section 2.2.4). Anomalies (between abrupt CO2 quadrupling and pre-industrial control) are computed as the difference between the mean of years 121-140 of *abrupt4xCO2* and the average of *piControl* simulations following Bjordal et al. (2020); Myers et al. (2021).

Satellite observations and reanalysis are used to constrain the LWP covariance with meteorology and the radiative covariance with LWP. Monthly-mean LWP is provided by the Multisensor Advanced Climatology of Liquid Water Path (MAC-LWP) (Elsaesser et al., 2017b). MAC synthesizes passive microwave observations of cloud LWP from multiple satellites. It provides 1° gridded total LWP output averaged over cloudy and cloud-free scenes, which makes it directly comparable to GCM LWP. However, microwave retrievals are only available over open water, which limits our ability to constrain the LWP response over sea ice.

Monthly-mean GMT and large-scale meteorology are described by Modern-Era Retrospective analysis for Research and Applications, Version 2 (MERRA-2) reanalysis (Gelaro, McCarty, Suárez, et al., 2017). LWP, GMT, and large-scale meteorology observations from 1992 to 2016 are used to test whether the chosen large-scale meteorology can predict observed LWP (section 3.1.1). The observed covariance between LWP and meteorology is used to constrain the GCM LWP response (section 3.1.2). Monthly-mean TOA SW fluxes are provided by the Clouds and the Earth’s Radiant Energy System (CERES) Energy Balanced and Filled (EBAF) Edition 4.1 product (Loeb et al., 2018b). The observed clear-sky flux in Edition 4.1 is adjusted to be consistent with the definition of GCM clear-sky flux (Loeb et al., 2020). The TOA SW fluxes and LWP from 2003 to 2016 are used to constrain the GCM radiative susceptibility (section 3.2) based on the availability of CERES and MAC-LWP data.

2.2 Methods

2.2.1 Simplified Physical Model for Predicting SW Cloud Feedback

In this work we seek to understand drivers of SW_{FB} . To this end, we develop a simplified physical model to predict the SO SW_{FB} . To give context to and motivate this analysis we provide a brief survey of the cloud and radiation response to warming in CMIP5 and CMIP6 GCMs. Figure 1a shows the SW_{FB} and LWP responses to increases in GMT for the GCMs surveyed in this study (written as $\Delta LWP/\Delta GMT$). Across GCMs, the LWP response is anti-correlated with model SW_{FB} and reproduces the dipole pattern of feedback in the SO (Figure 1b). GCMs with a larger increase in LWP in response to rising GMT tend to have more strongly negative SW_{FB} . While LWP generally increases with GMT, there are a few GCMs reporting decreasing LWP after the first few degrees of warming (Figure 1b). One goal of this study is to understand why these models behave differently from the majority of GCMs where LWP increases in step with GMT (section 3.1.3). This correspondence between LWP response to warming and SW_{FB} in the SO suggests that LWP can be used to describe how cloud macrophysical state drives cloud feedback in this region, consistent with previous studies (McCoy et al., 2022).

272 A simplified, but physical, model can be built to predict SW_{FB} based on the link-
 273 age between the change in liquid cloudiness and its effect on TOA radiative flux. SW_{FB}
 274 is the change in upwelling SW flux at TOA (ΔSW_{\uparrow}) due to the adjustment of cloud prop-
 275 erties, normalized by the change in GMT ($\Delta SW_{\uparrow C}/\Delta GMT$) (Zelinka, Myers, McCoy,
 276 Po-Chedley, et al., 2020). Because the downwelling SW flux at TOA (SW_{\downarrow}) is only a func-
 277 tion of months and latitudes, local SW_{FB} at a given month is proportional to the cloud-
 278 induced change in TOA albedo ($\alpha = SW_{\uparrow}/SW_{\downarrow}$) and normalized by GMT ($\Delta\alpha_C/\Delta GMT$).
 279 In turn, the response of α to warming can be approximated as the product of the sus-
 280 ceptibility of α to liquid ($\partial\alpha/\partial LWP$) and the response of cloud liquid to warming ($\Delta LWP/\Delta GMT$),
 281 as follows

$$282 \quad SW_{FB} = -\frac{\Delta SW_{\uparrow C}}{\Delta GMT} \propto -\frac{\Delta\alpha_C}{\Delta GMT} \sim -\frac{\partial\alpha}{\partial LWP} \cdot \frac{\Delta LWP}{\Delta GMT} \quad (1)$$

283 This model derives from previous work (McCoy et al., 2022). Equation 1 is used
 284 to predict GCM SW_{FB} calculated from radiative kernels (Zelinka, Myers, McCoy, Po-
 285 Chedley, et al., 2020). Equation 1 makes several simplifications based on the limitations
 286 of GCMs and observational data. Two simplifications central to the formulation of equa-
 287 tion 1 are detailed below.

288 First, SW_{FB} is proportional to $\Delta\alpha_C/\Delta GMT$ for a given latitude and time. As men-
 289 tioned in section 2.1, LWP observations are only available over open water, so we can
 290 not provide apples-to-apples observational constraints on the $\Delta LWP/\Delta GMT$ and $\partial\alpha/\partial LWP$
 291 for high latitudes. We average $\Delta LWP/\Delta GMT$ and $\partial\alpha/\partial LWP$ to allow regional con-
 292 straints.

293 Second, we neglect changes in albedo ($\Delta\alpha_C$) driven by changes in ice cloud in re-
 294 sponse to warming. We make this approximation for two reasons. First, there is no equiv-
 295 alent observational data set to MAC-LWP for IWP, making it difficult to offer an effec-
 296 tive observational constraint on the response of IWP to global warming. Second, IWP
 297 response (ΔIWP) to warming contributes minimally to a GCM SW_{FB} in this region
 298 (McCoy et al., 2022). This is due to a combination of the smaller magnitude of $\Delta IWP/\Delta GMT$
 299 compared to $\Delta LWP/\Delta GMT$ in the SO (McCoy et al., 2016) and the weaker scatter-
 300 ing of SW radiation per unit mass of ice compared to liquid due to the smaller size of
 301 typical liquid droplets relative to ice crystals (Liou, 2002; McCoy et al., 2014). Section
 302 3.3 evaluates the effect of neglecting ice on the results of this study.

303 As with any approximate model, the predictive ability of our model is degraded
 304 by the simplifications. The model in Equation 1 is balance between simplicity and ac-
 305 curacy. Uncertainty introduced by the simplifications will be reflected in the statistical
 306 uncertainty in the equation 1 prediction of GCM-derived SW_{FB} . This is similar to other
 307 studies seeking to develop a simplified, but interpretable, model that can explain vari-
 308 ability in the Earth system (Held & Soden, 2006; Qu et al., 2015). We constrain the SO
 309 SW_{FB} by providing constraints on the GCM LWP response ($\Delta LWP/\Delta GMT$) and the
 310 radiative susceptibility ($\partial\alpha/\partial LWP$) separately. Constraint methods are discussed in the
 311 following sections.

312 **2.2.2 Prediction of LWP using Cloud-Controlling Factor Analysis**

313 In this section we examine the linkage between LWP and large-scale meteorology.
 314 The large-scale environmental factors affecting local cloud properties are referred to as
 315 cloud-controlling factors (Stevens & Brenguier, 2009). CCF analysis is based on the idea
 316 that the response of cloud properties to global warming can be expressed by a first-order
 317 Taylor expansion in CCFs (Klein et al., 2017). One application of this framework in the
 318 literature is to use observations to constrain LWP response to GCM-predicted changes

319 in CCFs (Qu et al., 2015; Klein et al., 2017). Following Qu et al. (2015), we predict the
 320 response of LWP to GMT as

$$321 \quad \frac{\Delta LWP}{\Delta GMT} = \sum_i \frac{\partial LWP}{\partial X_i} \frac{\Delta X_i}{\Delta GMT} + Res \quad (2)$$

322 where X_i are CCFs. Equation 2 decomposes LWP response to GMT into the LWP re-
 323 sponses to CCFs and a residual term. LWP response to GMT induced by each CCF is
 324 a product of the sensitivity of LWP to each CCF ($\partial LWP/\partial X_i$) and the response of that
 325 CCF to GMT ($\Delta X_i/\Delta GMT$). The CCF model shown in equation 2 is trained on *piControl*
 326 simulations of each GCM to calculate $\partial LWP/\partial X_i$. The $\Delta X_i/\Delta GMT$ term is given by
 327 the differences between *piControl* and *abrupt4xCO₂* simulations of each GCM. Com-
 328 pared to clouds, CCFs suffer from less parametric uncertainty in GCMs because they
 329 are aspects of the resolved large-scale processes (Qu et al., 2015; Klein et al., 2017). Us-
 330 ing equation 2, we can provide a constraint on the LWP response to GMT by replacing
 331 the $\partial LWP/\partial X$ derived from *piControl* simulations of GCMs with the values derived
 332 from observations and using GCM estimates of $\Delta X_i/\Delta GMT$. As discussed in the in-
 333 troduction, an important assumption underlying CCF analysis is that the relationships
 334 between clouds and CCFs are time-scale invariant (Qu et al., 2015; Klein et al., 2017).
 335 We test this assumption in section 3.1.

336 The CCFs (X_i) considered in this study are surface skin temperature (T_s), precip-
 337 itation minus evaporation ($P-E$), lower tropospheric stability (*LTS*) (Klein & Hart-
 338 mann, 1993; Slingo, 1980), and 500 mb subsidence (ω_{500}). These CCFs are consistent
 339 with previous studies of covariance between extratropical clouds and meteorology (McCoy,
 340 Field, Bodas-Salcedo, et al., 2020; McCoy et al., 2022; Zelinka, Myers, McCoy, Po-Chedley,
 341 et al., 2020; Zelinka et al., 2018).

342 We use $P-E$ as a proxy for moisture convergence because moisture convergence
 343 is not output from GCMs participating in CMIP5 and CMIP6. These two terms differ
 344 by the change in moisture storage over time (Seager & Henderson, 2013). To demonstrate
 345 that these quantities are nearly identical for our study, we examine the fifth generation
 346 European Centre for Medium-Range Weather Forecasts (ECMWF; ERA5) for both vari-
 347 ables, $P-E$ is a close approximation of moisture convergence in $40-85^\circ S$ when we
 348 averaged them in $5^\circ \times 5^\circ$ gridbox of monthly output (Figure S1 in the supplementary
 349 information). The discrepancy between these two variables in GCMs should be smaller
 350 than in reanalysis because of the absence of an analysis increment in GCMs (Seager &
 351 Henderson, 2013). For these reasons, we will average GCM LWPs and CCFs as well as
 352 observations over $5^\circ \times 5^\circ$ gridboxes within $40-85^\circ S$ to conduct the CCF analysis. The
 353 LWP response is predicted by the CCF model (Equation 2) in each $5^\circ \times 5^\circ$ gridbox in
 354 the SO.

355 $P-E$ is consistently positive in $40-85^\circ S$ across all GCMs in the mean state cli-
 356 mate (*piControl* simulation) (gray lines in Figure S2). In *abrupt4xCO₂* simulations, $P-E$
 357 reduces in the $40-50^\circ S$ region and enhances across the $50-85^\circ S$ region (colored
 358 lines in Figure S2). This is consistent with a poleward expansion of subtropical drying
 359 region under global warming (Siler et al., 2018; Bonan et al., 2023) and a robust moist-
 360 ening of latitudes poleward of $50^\circ S$ (Held & Soden, 2006). Comparing moisture conver-
 361 gence response to warming and SW_{FB} suggests that $50^\circ S$ may act as a demarcation be-
 362 tween positive SW_{FB} (negative $\Delta LWP/\Delta GMT$) and negative SW_{FB} (positive $\Delta LWP/\Delta GMT$)
 363 estimated from *abrupt4xCO₂* simulations of CMIP5 and CMIP6 GCMs (Figure 1a) due
 364 to changes in moisture convergence regime. This is consistent with the notion that the
 365 hydrological response to warming (Held & Soden, 2006) sets some of the pattern of SW
 366 cloud feedback in the SO (McCoy et al., 2022). To characterize this feature, we present
 367 our analysis separately for the $40-50^\circ S$ and $50-85^\circ S$ regions (sections 3.1.2 and 3.3).

368 We use monthly-mean data to examine the covariance between LWP and $P - E$.
 369 This enables averaging across the synoptic systems that drive extratropical moisture con-
 370 vergence (Field & Wood, 2007). This approach is not particularly new and many pre-
 371 vious studies have leveraged monthly mean CCFs to predict extratropical cloudiness (Zelinka,
 372 Myers, McCoy, Po-Chedley, et al., 2020; Zelinka et al., 2018; Ceppi, McCoy, & Hartmann,
 373 2016). We believe this averaging doesn't substantially degrade our results based on pre-
 374 vious studies relating LWP in extratropical cyclones to moisture convergence (McCoy
 375 et al., 2019; McCoy, Field, Bodas-Salcedo, et al., 2020). We don't expect that monthly
 376 averages will strongly degrade the predictive capacity of our CCF model since previous
 377 studies examining daily means suggest fairly linear dependence of LWP on CCFs (McCoy
 378 et al., 2018; McCoy, Field, Bodas-Salcedo, et al., 2020). We test whether performing our
 379 analysis on monthly means degrades the predictive ability of our model using two out-
 380 of-sample tests.

381 *2.2.3 Cloud Regime Temperature-dependence*

382 CCF analysis has been used in numerous studies to predict the response of clouds
 383 to warming in the tropics and subtropics (Qu et al., 2015; Zhai et al., 2015; Myers & Nor-
 384 ris, 2016; Brient & Schneider, 2016; McCoy et al., 2017; Myers et al., 2021; Wall et al.,
 385 2022) as well as the extratropics (Ceppi, McCoy, & Hartmann, 2016; Zelinka, Myers, Mc-
 386 Coy, Po-Chedley, et al., 2020; Zelinka et al., 2018). The SO region present a challenge
 387 to a CCF model that lumps together all clouds into a single set of sensitivities between
 388 clouds and CCFs (i.e, equation 2). From $40 - 85^\circ S$, T_s varies from $210 K$ in the aus-
 389 tral winter over the Antarctic continent to around $290 K$ in the summer subtropics. The
 390 temperature of the atmosphere and clouds varies along with T_s . The wide range of cloud
 391 temperatures results in a combination of mixed-phase clouds and liquid-only clouds in
 392 the SO (Tan et al., 2016).

393 The formation and removal processes governing liquid and mixed-phase clouds are
 394 very different (Morrison et al., 2012). Precipitation efficiency is higher in mixed-phase
 395 clouds than in liquid-only clouds due to the rapid growth of ice crystals at the expense
 396 of liquid drops (Storelvmo & Tan, 2015). The higher precipitation efficiency of mixed-
 397 phase clouds results in the majority of mid-latitude precipitation events originating as
 398 snow (Field & Heymsfield, 2015). Previous studies suggest that mixed-phase and liquid-
 399 only clouds will respond differently to global warming (Tan et al., 2016). GCM low cloud
 400 optical depth increases with warming for cold clouds and decreases with warming for warm
 401 clouds (Gordon & Klein, 2014; Terai et al., 2016). This behavior is also found in in-situ
 402 observations (Terai et al., 2019).

403 Because of the differing cloud physics and potential cloud feedback processes aris-
 404 ing due to cold (mixed-phase) and warm (liquid-only) clouds, we split our CCF model
 405 over temperature. The intent of splitting our CCF model over temperature is to sepa-
 406 rate the SO into regions that are only mixed-phase and only liquid-only clouds, which
 407 is not really possible in the context of climate model output at monthly resolution, but
 408 to separate the SO into regimes that are dominated by different processes and therefore
 409 LWP covaries with CCFs differently. We count a $5^\circ \times 5^\circ$ gridbox in $40-85^\circ S$ as a cold
 410 (warm) regime gridbox if the mean T_s of gridbox is lower than (larger or equal to) a thresh-
 411 old T_s (TR_{T_s}). This results in a CCF model split over TR_{T_s} :

$$\begin{aligned}
\frac{\Delta LWP}{\Delta GMT}|_{Cold} &= \sum_i \left(\frac{\partial LWP}{\partial X_i}|_{Cold} \cdot \frac{\Delta X_i}{\Delta GMT}|_{Cold} \right) + Res_1 \\
& T_s < TR_{T_s} \\
\frac{\Delta LWP}{\Delta GMT}|_{Warm} &= \sum_i \left(\frac{\partial LWP}{\partial X_i}|_{Warm} \cdot \frac{\Delta X_i}{\Delta GMT}|_{Warm} \right) + Res_2 \\
& T_s \geq TR_{T_s}
\end{aligned} \tag{3}$$

412

413

414

415

416

417

418

419

420

421

422

423

424

425

426

427

428

429

430

431

432

433

We have two goals in our methodology for determining TR_{T_s} for each GCM. First, we want to make the determination of TR_{T_s} objective for each GCM. Second, we want to make the determination of TR_{T_s} in a way that allows an analogous calculation for observations. For each GCM, TR_{T_s} is defined as the threshold T_s that maximizes the explained variance in mean-state (*piControl*) LWP by the CCF model in equation 3. For each GCM we iterate through possible TR_{T_s} values within the entire range of T_s within the SO latitudes and calculate the coefficient of determination (R^2) of equation 3 when predicting *piControl* LWP (Figure S3 in the supplementary information). Equation 3 explains more than 70 % of the variance of *piControl* LWP across GCMs. One question is whether TR_{T_s} is time scale invariant. In Figure S4 of the supplementary information, we calculate TR_{T_s} using *abrupt4xCO2* data instead of *piControl*. The TR_{T_s} trained using *abrupt4xCO2* simulations correlates with TR_{T_s} trained from *piControl* simulations, supporting that TR_{T_s} is time-scale invariant. We use the TR_{T_s} trained on *piControl* simulations to predict the LWP response to warming in *abrupt4xCO2* simulations (section 3.1.2). The TR_{T_s} for most GCMs is around 270 K (Figure S3), which generally separates the clouds over cold ice or land surfaces from the open ocean. Komurcu et al. (2014) shows that the supercooled liquid fraction in GCMs dramatically drops when cloud temperature is lower than 255 K. Assuming a typical extratropical environment with cloud base height of 2–3 km and lapse rate of 6.5 K/km, its T_s would be close to 270 K. This is consistent with the idea that mixed-phased and liquid-only clouds have different cloud physics and response behaviors to their environments.

434

435

436

437

438

439

Because microwave radiometers do not retrieve LWP over ice (Elsaesser et al., 2017b), we need to consider sampling differences between GCMs and observations when providing observational constraints. The region for which valid data is available from MAC is very similar to GCM warm regimes (Figure S5). In the remainder of this study observational constraint is only available for the warm regime of equation 3 and all the cold regime observations are treated missing due to lack of observations.

440

2.2.4 Radiative Susceptibility

441

442

443

444

In equation 1, the response of LWP to GMT is connected to its SW radiative effect through a radiative susceptibility term ($\partial\alpha/\partial LWP$). This term describes how a change in LWP affects α while keeping other factors fixed. Following McCoy et al. (2022), the radiative susceptibility is estimated by training the multi-linear regression model

445

$$\alpha = c_1 * LWP + c_2 * \alpha_{clear-sky} + c_3 \tag{4}$$

446

447

448

449

450

451

452

453

454

where c_1 is $\partial\alpha/\partial LWP$. The regression model is trained on *piControl* GCM simulations and observations to obtain radiative susceptibilities for GCMs and observations. Training is performed at the native spatial resolution of the data. TOA albedo α is a function of clear-sky albedo (α_{cs}) and LWP, while LWP is in turn affected by cloud areal extent (Bender et al., 2017) and cloud optical depth (Gordon & Klein, 2014). By including α_{cs} as a predictor we seek to separate the change in α contributed by changes in clouds from non-cloud perturbations (e.g., surface conditions). This is consistent with calculating SW_{FB} by adjusting the SWCRE response for non-cloud influences using radiative kernels (Zelinka, Myers, McCoy, Po-Chedley, et al., 2020; Soden et al., 2008).

One way to think of equation 4 is a very simple radiative kernel. To enable the use of equation 4 we subset our training data to remove cases where surface albedo or near surface sun angle strongly affect TOA albedo. The sensitivity of TOA upwelling SW flux to changes in cloudiness over a bright surface is low because of the high surface albedo. Consequently SW_{FB} is nearly zero over surface ice (i.e. the Antarctic continent) (Shell et al., 2008). We train equation 4 over open water to minimize the effect of extremely bright surfaces on the calculation of $\partial\alpha/\partial LWP$. We subset training data using a clear-sky albedo threshold ($TR_{\alpha_{cs}}$). We evaluate the sensitivity of $\partial\alpha/\partial LWP$ to the value of $TR_{\alpha_{cs}}$ in section 3.2. Increasing solar zenith angle increases albedo (McCoy et al., 2018). Compounding this effect, LWP decreases in winter while solar zenith angle increases. Data from a single month is used to calculate the radiative susceptibility $\partial\alpha/\partial LWP$ to reduce the effects of spurious covariation between solar zenith angle and LWP. We choose January because austral summer is the time that the change in LWP contributes the most to SW_{FB} when insolation is strong.

3 Results

3.1 Predicting LWP

The first step to providing an observational constraint on SW_{FB} using equation 1 is to constrain the response of SO LWP to warming using observed covariability between CCFs and LWP. To understand the uncertainty in our CCF-based constraint of LWP response we need to evaluate whether the relationships between LWP and CCFs are invariant across time scales (Klein et al., 2017). Two out-of-sample tests are performed to test time scale invariance, and more broadly, to test the predictive skill of the CCF model. First, we train a CCF model (equation 2) on monthly-mean observations for a short period and use it to predict the interannual variability of LWP back to 1992. This is shown in section 3.1.1. Second, we train the regression model in equation 3 on monthly-mean *piControl* simulations and use it to predict the GCM-simulated response of LWP to CO_2 quadrupling. This is discussed in section 3.1.2. Following these tests, we use the LWP-CCF relationships obtained from observations to constrain the LWP responses in GCMs in section 3.1.2. In section 3.1.3, we discuss GCM LWP responses by apportioning $\Delta LWP/\Delta GMT$ among the CCFs.

3.1.1 Predicting Historical Trends in LWP

Observations of LWP are available from 1992-2016. We split this period into a training period (2012-2016) and a validation period (1992-2011). Equation 2 is trained on 2012-2016 to calculate $\partial LWP/\partial X_i$. Equation 2 is used to predict the interannual variation of LWP 1992-2011. MAC-LWP observes an increase in SO LWP over the past two decades, consistent with Manaster et al. (2017) and Norris et al. (2016) (Figure 2a). The predicted LWP from equation 2 broadly reproduces the positive trend of LWP during the period from 1996 onward (Figure 2a). Before 1996, the LWP trend predicted by the CCF model is negative. This may be because the CCFs predicted by MERRA-2 are reliant on the observations being ingested into the reanalysis. Many fewer observations of precipitation are available before the mid-1990s (Gelaro, McCarty, Suárez, et al., 2017). The lack of observational input to reanalysis may lead to the disagreement between the LWP predicted by the CCF model and LWP observations in the early 1990s. During the period where numerous observations were available to the MERRA-2 reanalysis, the ability of CCF model in equation 2 to reproduce the decadal-scale trend and interannual variability of LWP in an out-of-sample test supports the time-scale invariance of $\partial LWP/\partial X_i$. The ability of the CCF model to reproduce the observed trend in LWP is not sensitive to the choice of training and validation periods (Figure S6).

Equation 2 can be used to decompose the predicted trend into contributions from individual CCFs. The positive decadal trend in SO LWP can be largely explained by the

505 increase in $P-E$ (Figure 2b). Increases in T_s explain only a small fraction of the LWP
 506 trend. Stability and large-scale subsidence have negligible effects on the SO LWP on a
 507 decadal scale. Increased $P-E$ is related to the increased moisture content in the ex-
 508 tratropical atmosphere (Held & Soden, 2006). This result suggests that the hydrolog-
 509 ical cycle has played an important role in the response of SO LWP to increased GMT
 510 over the past two decades (Norris et al., 2016; Manaster et al., 2017).

511 **3.1.2 Predicting LWP response to CO_2 Quadrupling**

512 Following our evaluation of time-scale invariance of $\partial LWP/\partial X_i$ in observations,
 513 we evaluate whether the $\partial LWP/\partial X_i$ trained using *piControl* GCM data can be used
 514 to predict the LWP response in *abrupt4xCO₂* simulations. Figure 3 shows the changes
 515 in LWP in response to warming ($\Delta LWP/\Delta GMT$) between the average of *piControl* and
 516 the mean of years 121-140 of *abrupt4xCO₂* simulations (Myers et al., 2021; Bjordal et
 517 al., 2020). Predicted LWP responses are shown in three latitude bands: 40–85°S (Fig-
 518 ure 3 left); 40–50°S (Figure 3 middle); and 50–85°S (Figure 3 right). The CCF model
 519 (equation 3) predicts 70% of GCM variance in $\Delta LWP/\Delta GMT$ in the latitude band en-
 520 compassing the SO (Figure 3b). This supports the time-scale invariance of $\partial LWP/\partial X_i$.
 521 The explained variance in the 40–50°S latitude band is 60% (Figure 3d). This decrease
 522 in explained variance relative to the entire SO may be related to the hydrological response
 523 in this region. While moisture is converged into 40–50°S in the mean-state climate,
 524 the convergence pattern becomes less robust at the end of *abrupt4xCO₂* simulations. Some
 525 GCMs display drying and some display moistening in 40–50°S (Figure S2). In the lat-
 526 itude band where warming simulations consistently predict moistening (50–85°S), the
 527 explained variance in $\Delta LWP/\Delta GMT$ is 86% (Figure 3f).

528 Because observational constraint from MAC-LWP is only available in the warm regime,
 529 we separate the predictions of CCF model into warm and cold regimes for each latitude
 530 band. The LWP response to GMT in the warm regime predicts the majority of total LWP
 531 response across latitude bands (Figure 3ace). Only the warm regime exists in the 40–
 532 50°S region, so $r^2 = 1$ (Figure 3c). The explained variance in $\Delta LWP/\Delta GMT$ by warm
 533 regime is still high in the 50–85°S region ($r^2 = 0.64$, Figure 3e).

534 We calculate how observations in the warm regime in each latitude band constrain
 535 overall $\Delta LWP/\Delta GMT$. The $\partial LWP/\partial X_i$ for each GCM in the warm regime is replaced
 536 with the $\partial LWP/\partial X_i$ computed from observations yielding a constraint on $\Delta LWP/\Delta GMT$
 537 in the warm regime. This constraint is propagated from the warm regime to the aggre-
 538 gate of both regimes. Uncertainty in the best fit line fit relating the CCF prediction of
 539 the warm regime to the CCF prediction of both regimes is estimated by Jackknife re-
 540 sampling (Tukey, 1958). We intersect the shaded regions on the x-axis in Figure 3ace
 541 with the best-fit lines and their uncertainties to propagate the warm regime constraint
 542 to both regimes for each latitude band. The observational constraint on $\Delta LWP/\Delta GMT$
 543 for each latitude band is then propagated through the uncertainty from the CCF model.
 544 In Figure 3bdf, the constrained ranges from the y-axis of Figure 3ace are denoted via
 545 intersection of the brown shading with the x-axis. The best fit lines and uncertainty in
 546 Figure 3bdf are used to propagate the constraints on the CCF model predictions to the
 547 GCM simulated LWP response. These constraints are used in section 3.3 to constrain
 548 SW_{FB} . Once propagated, observational constraints on the warm regime point towards
 549 a moderate $\Delta LWP/\Delta GMT$ across the SO.

550 Potential systematic biases in the passive microwave observations of LWP can be
 551 propagated to uncertainty in our constraint on $\Delta LWP/\Delta GMT$. Observational biases
 552 in LWP impact constraints on $\Delta LWP/\Delta GMT$ by affecting the observed sensitivities
 553 of LWP to CCFs ($\partial LWP/\partial X$). Potential systematic biases in microwave LWP obser-
 554 vations are estimated following Greenwald et al. (2018). The net bias of LWP in the SO
 555 (poleward to 40°S) should be smaller than +10 g/m^2 and is relatively spatially uniform

(Figure 17(f) and Figure 19(a) in Greenwald et al. (2018)). The LWP percentage bias is $\pm 10.8\%$, calculated by dividing $\pm 10 \text{ g/m}^2$ by the averaged LWP during the observational training period. We then recalculate $\partial LWP/\partial X_i$ by perturbing the observational values of LWP by $\pm 10.8\%$. Considering potential observational LWP bias slightly loosens the constraint of $40\text{--}85^\circ S \Delta LWP/\Delta GMT$ from $[2.76, 4.19] \text{ g m}^2 \text{ K}^{-1}$ to $[2.60, 4.47] \text{ g m}^2 \text{ K}^{-1}$. The effect of observational bias is propagated through to the constraint on the SO SW_{FB} in section 3.3.

3.1.3 CCF Contributions to LWP Response to CO_2 Quadrupling

In this section we show the sensitivities of LWP to CCFs ($\partial LWP/\partial X_i$) as well as each CCF's contribution to the LWP response to warming following similar analysis in previous studies (Zelinka, Myers, McCoy, Po-Chedley, et al., 2020). $\partial LWP/\partial X_i$ for each GCM (Figure 4a) can be scaled by the change in each CCF between *piControl* and the end of *abrupt4xCO₂* simulation ($\Delta X_i/\Delta GMT$; Figure 4b) to yield the contribution of each CCF to $\Delta LWP/\Delta GMT$ (Figure 4c; equation 3). Cold and warm regime predictions are shown separately. Observed $\partial LWP/\partial X$ are only available for the warm regime (Figure 4a).

The dependence of LWP on CCFs across GCMs and observations (Figure 4a) is broadly consistent with previous studies. The coefficient relating LWP and T_s ($\partial LWP/\partial T_s$) is positive across all GCMs for the cold regime. Agreement between GCMs on the sign of $\partial LWP/\partial T_s$ decreases for the warm regime. This is consistent with previous studies suggesting that cold cloud optical depth increases in response to warming (Gordon & Klein, 2014; Terai et al., 2019), mostly due to the increased cloud water content (Betts & Harshvardhan, 1987). Terai et al. (2019) suggests that the cloud optical depth for warm clouds may decrease or stay constant with increasing temperature owing to the reduced cloud adiabaticity. The coefficient relating LWP to $P - E$ ($\partial LWP/\partial P - E$) is positive for warm and cold regimes, which is consistent with previous literature (McCoy et al., 2019; McCoy, Field, Bodas-Salcedo, et al., 2020). The coefficient relating LWP and LTS ($\partial LWP/\partial LTS$) is mostly positive in the warm regime of GCMs, while the coefficient relating LWP to ω_{500} ($\partial LWP/\partial \omega_{500}$) is small. This is consistent with previous work on boundary layer cloudiness (Zelinka et al., 2018; Myers & Norris, 2015, 2013). Observed $\partial LWP/\partial T_s$ and $\partial LWP/\partial P - E$ are positive and much larger than $\partial LWP/\partial LTS$ and $\partial LWP/\partial \omega_{500}$.

Both T_s and $P - E$ increase with warming in warm and cold regimes (Figure 4b). LTS increases with warming in the warm regime but decreases in the cold regime. This pattern may be related to the poleward shift of the Hadley cell (stabilizing the warm regime lower troposphere) and the poleward shift of the Southern Hemisphere storm track (destabilizing the cold regime lower troposphere) simulated by GCMs (Barnes & Polvani, 2013; Bender et al., 2012). The variation in large-scale subsidence is relatively small compared to other CCFs.

Combining $\partial LWP/\partial X_i$ and the response of CCF to warming ($\Delta X_i/\Delta GMT$) allows us to apportion $\Delta LWP/\Delta GMT$ among CCFs. In the warm regime, GCMs have roughly equivalent contributions due to T_s , $P - E$, and LTS . In the cold regime, $P - E$ and T_s changes contribute the most (Figure 4c).

Among the GCMs surveyed here (Table S1), the second Community Earth System Model (CESM2), its variants (CESM2-WACCM, CESM2-FV2, CESM2-WACCM-FV2), and E3SM-1-0 predict a decrease in LWP after the first few degrees of warming in *abrupt4xCO₂* simulations (Figure 1b), which is consistent with previous studies (Bjorndal et al., 2020). These models share a similar atmosphere component (Danabasoglu et al., 2020; Golaz et al., 2019; Rasch et al., 2019). Focusing on CESM2 in Figure 4, characterizes how decreases in LWP as GMT increases relate to CCFs. The prediction of CESM2's LWP response to warming by equation 3 trained on *piControl* is less skillful than the prediction for other GCMs (Figure S7), but it is improved relative to previous CCF-based pre-

607 dictions (McCoy et al., 2022). While work is required to more accurately predict the CESM2
 608 LWP response using a CCF model, the decreased LWP in the warm regime is captured
 609 by equation 3 (Figure 4c and Figure S7). Decomposing the prediction from equation 3
 610 suggests that the LTS-induced increase in CESM2 LWP in the warm regime is offset by
 611 decreases related to T_s . CESM2 displays the lowest warm regime $\partial LWP/\partial P - E$ and
 612 the $P - E$ contribution to LWP response is small (Figure 4ac). Relative to observations
 613 CESM2 overestimates $\partial LWP/\partial LTS$ and underestimates $\partial LWP/\partial P - E$ in the warm
 614 regime. Warm regime $\partial LWP/\partial T_s$ is negative in CESM2, but is positive in observations
 615 (Figure 4a). Warm regime T_s , $P - E$, and LTS increase in response to GMT (Figure
 616 4b) and the net effect is a negative trend in LWP beyond the first degree of warming with
 617 an the overall near-zero response of LWP to warming.

618 As mentioned in the introduction, the phase shift in mixed-phased clouds is one
 619 of the potential mechanisms that may contribute to the increase in SO LWP that in turn
 620 drives a negative SW_{FB} (Tan et al., 2016). Bjordal et al. (2020) attribute the high cli-
 621 mate sensitivity of CESM2 to its large mean-state supercooled liquid fraction (i.e., small
 622 ice fraction) in the SO because its low-level clouds are easily shifted to being liquid-dominated
 623 and the contribution of the negative cloud phase feedback reduces as GMT increases.
 624 We examine this idea in the context of our analysis framework by examining the state
 625 dependence of $\partial LWP/\partial T_s$. In the context of our CCF model, $\partial LWP/\partial T_s$ may indicate
 626 the contribution to LWP change by shifts between ice and liquid. As with any other cor-
 627 relative analysis caution should be used in interpreting this metric since it may also re-
 628 lated to other processes such as shifts in the moist adiabat.

629 Following Bjordal et al. (2020), we calculate $\partial LWP/\partial T_s$ in 15-year chunks dur-
 630 ing the 150 years of *abrupt4xCO2* simulations to contrast how this sensitivity evolves
 631 with warming across GCMs (Text S1). We find that CESM2 is an outlier among the GCMs
 632 surveyed here in regards to how $\partial LWP/\partial T_s$ changes with time (Figure S8 in the sup-
 633plementary information). $\partial LWP/\partial T_s$ shifts toward more negative values as warming
 634 continues. This behavior is not displayed in other GCMs. This is consistent with the anal-
 635 ysis of CESM2 in Bjordal et al. (2020). For GCMs like CESM2 that have large super-
 636 cooled liquid fractions, as the climate warms the ice available for transition to liquid is
 637 decreased and the phase shift-related changes in LWP are reduced. This may explain the
 638 non-monotonic response of LWP to warming that is displayed in CESM2.

639 3.2 Radiative Susceptibility

640 Following equation 1, we argue that SW_{FB} can be approximated as proportional
 641 to the product of change in LWP and the sensitivity of albedo to LWP. Across GCMs,
 642 $\partial\alpha/\partial LWP$ vary by nearly a factor of seven. One emergent behavior in GCMs is an in-
 643 verse relationship between $\partial\alpha/\partial LWP$ and mean-state LWP. This is consistent with pre-
 644 vious studies (McCoy et al., 2022). TOA albedo and cloud fraction (areal coverage of
 645 clouds) are approximately linearly related until the scene becomes overcast (Bender et
 646 al., 2017). The effect of in-cloud LWP on albedo saturates at high in-cloud LWP (Lacis
 647 & Hansen, 1974). The SO mean-state LWP is a function of cloud fraction and in-cloud
 648 LWP. A GCM that simulates high mean-state LWP has fewer clear-sky pixels that can
 649 be filled and is closer to radiative saturation. As LWP increases with warming, additional
 650 liquid affects α less efficiently by only increasing the in-cloud liquid rather than increas-
 651 ing cloud coverage.

652 Radiative susceptibility calculated from CERES and MAC-LWP observations is
 653 low relative to GCMs (Figure 5). This result suggests that the too-bright and too-homogeneous
 654 bias of tropical clouds in CMIP6 GCMs (Konsta et al., 2022) may also exist in the sim-
 655 ulation of extratropical clouds. One potential uncertainty in estimating $\partial\alpha/\partial LWP$ is
 656 the clear-sky albedo threshold ($TR_{\alpha_{cs}}$) applied before training the regression model in
 657 equation 4. We include this uncertainty in the SW_{FB} constraint by calculating $\partial\alpha/\partial LWP$

658 varying $TR_{\alpha_{cs}}$ from 0.11 to 0.30 (0.105 is lowest clear-sky albedo for some GCMs). This
 659 uncertainty range is compounded by potential systematic uncertainty in observed LWP
 660 as discussed above. When both sources of uncertainty are included, the range of observed
 661 susceptibility widens from $[0.43, 0.90] (kg\ m^{-2})^{-1}$ to $[0.39, 1.01] (kg\ m^{-2})^{-1}$.

662 One intriguing feature of GCMs is that GCMs where SO LWP is more sensitive
 663 to the hydrological cycle (large $\partial LWP/\partial P - E$) tend to have a weaker radiative response
 664 (small $\partial\alpha/\partial LWP$). This results in a buffering between macrophysical cloud response
 665 to GMT and radiative response to GMT. We examine how radiative and macrophysical
 666 factors are linked through mean-state LWP. $\partial LWP/\partial P - E$ positively correlates with
 667 mean-state LWP in both cold and warm regimes (Figure 5). This relationship can be
 668 explained in the context of sources and sinks of cloud liquid content (McCoy, Field, Bodas-
 669 Salcedo, et al., 2020; McCoy et al., 2022). Source and sink rates of clouds can be writ-
 670 ten as

$$671 \begin{aligned} K_{source} &= e_{source} \cdot r_{water\ vapor} \\ K_{sink} &= e_{sink} \cdot r_{LWP} \end{aligned} \quad (5)$$

672 with rates being the product of bulk efficiency coefficients for sources (e_{source}) and sinks
 673 (e_{sink}) and their respective reservoir terms. The reservoir that liquid draws from is wa-
 674 ter vapor ($r_{water\ vapor}$) while the sink reservoir (precipitation) is cloud liquid (r_{LWP}).
 675 In the mean-state climate, sources and sinks are balanced ($K_{source} = K_{sink}$) and

$$676 \frac{e_{source}}{e_{sink}} = \frac{r_{LWP}}{r_{water\ vapor}}. \quad (6)$$

677 Following this conceptual model, mean-state LWP is proportional to the relative strength
 678 of source and sink efficiencies (i.e., e_{source}/e_{sink}). If we assume the same water vapor
 679 ($r_{water\ vapor}$) in the mean-state climates of GCMs, the diversity in model mean-state LWP
 680 can be traced back to the subgrid-scale parameterization of cloud source and sink pro-
 681 cesses. Similarity in water vapor climatologies is an assumption, since free-running mod-
 682 els without a fixed SST will yield slightly different mean-state water vapor paths (Jiang
 683 et al., 2012). In this conceptual model $\partial LWP/\partial P - E$ trained using the GCM mean-
 684 state climate may act as a proxy for the relative strength of source to sink efficiencies
 685 ($e_{source}/e_{sink} \propto \partial LWP/\partial P - E$).

686 The steady-state framework outlined here provides insight into why the slope of
 687 $\partial LWP/\partial P - E$ for the cold regime is larger than the slope for the warm regime (Fig-
 688 ure 5). In this framework, differences in slope could arise due to a stronger source effi-
 689 ciency for cold regime clouds due to the larger moist adiabat (Betts & Harshvardhan,
 690 1987), even though the sink efficiency for cold regime clouds may be larger as well (Field
 691 & Heymsfield, 2015)

692 How does the steady-state framework outlined above inform us of the diversity in
 693 the GCM LWP responses to warming? The moisture content ($r_{water\ vapor}$) in the ex-
 694 tratropics increases with GMT. If we assume the relative strength of source-to-sink ef-
 695 ficiency (e_{source}/e_{sink}) is fixed under climate change, a model with larger mean-state sen-
 696 sitivity of LWP to $P - E$ would simulate a larger increase in LWP. This is consistent
 697 with GCM behavior and warm regime $\partial LWP/\partial P - E$ and $\Delta LWP/\Delta GMT$ covary across
 698 GCMs (Figure S9 in the supplementary information) with a correlation of $r = 0.78$.

699 3.3 Constraints on Southern Ocean SW Cloud Feedback

700 In the proceeding sections we examine the response of SO LWP to GMT predicted
 701 by CCFs and the response of α to LWP. Combining these terms in equation 1 we eval-
 702 uate whether our simplified model of SW_{FB} has skill in predicting GCM SW_{FB} . In Fig-
 703 ure 6, we use the $\Delta LWP/\Delta GMT$ and $\partial\alpha/\partial LWP$ calculated from GCMs to predict their
 704 SW_{FB} calculated using radiative kernels as presented in Zelinka, Myers, McCoy, Po-Chedley,

et al. (2020). The ability of the simple model in equation 1 to reproduce SW_{FB} is evaluated in the $40 - 50^\circ S$ and $50 - 85^\circ S$ latitude bands (Figure 6). Equation 1 explains 54 % of the variance in GCM SW_{FB} averaged over $40 - 50^\circ S$ and 40 % averaged over $50 - 85^\circ S$.

Based on the observational constraints on $\Delta LWP/\Delta GMT$ (Figure 3) and the observational estimate of $\partial\alpha/\partial LWP$ (Figure 5), we provide observational constraints on SW_{FB} . Observational constraints on the right-hand side of equation 1 predict the contributions of $40 - 50^\circ S$ and $50 - 85^\circ S$ regions' clouds to global mean cloud feedback to be $0.00 - 0.06 W m^{-2} K^{-1}$ and $-0.15 - 0.01 W m^{-2} K^{-1}$. These ranges are calculated by taking the shaded y-ranges in Figure 6 and scaling them by the ratio of the area in the latitude band to global surface area. The constraint on $50 - 85^\circ S$ SW_{FB} is consistent with the constraint $-0.10 - 0.0 W m^{-2} K^{-1}$ calculated by McCoy et al. (2022). The uncertainties in $40 - 50^\circ S$ and $50 - 85^\circ S$ SW_{FB} constraints are calculated by combining uncertainties in $\Delta LWP/\Delta GMT$ constraints and the uncertainty in the estimate of $\partial\alpha/\partial LWP$. Uncertainties in the constraints on $\Delta LWP/\Delta GMT$ are due to the intermodel spread in $\Delta X/\Delta GMT$ and the uncertainties propagated from the warm regime to latitude bands including both cold and warm regimes (section 3.1.2). The uncertainty in $\partial\alpha/\partial LWP$ is given by varying the clear-sky albedo threshold (section 3.2). The constraint on $40 - 50^\circ S$ SW_{FB} is tighter than for $50 - 85^\circ S$ because an observational constraint on $\Delta LWP/\Delta GMT$ is only available in the warm regime, and the $40 - 50^\circ S$ region is entirely within the warm regime.

To evaluate the extent to which neglecting ice water path (IWP) changes impact our prediction of GCM SW_{FB} , we examined the relative contributions of LWP and IWP changes to SW_{FB} in GCMs. We first calculate the changes in IWP with GMT ($\Delta IWP/\Delta GMT$) between the mean of years 121-140 of *abrupt4xCO2* and the average of *piControl* simulations for all GCMs in this study following the same procedure used in the calculation of $\Delta LWP/\Delta GMT$. The median $\Delta LWP/\Delta GMT$ in $40 - 85^\circ S$ is around 10 times larger than $\Delta IWP/\Delta GMT$ across GCMs (Figure S10a). To compare the sensitivity of albedo to LWP ($\partial\alpha/\partial LWP$) with IWP ($\partial\alpha/\partial IWP$), we first partition the TOA albedo (α) into 50 LWP/IWP bins. Then we follow the method for calculating radiative susceptibility (section 2.2.4) to compute the sensitivities of albedo to liquid versus ice by keeping the other variable fixed (Text S2). The product of $\partial\alpha/\partial LWP$ ($\partial\alpha/\partial IWP$) and $\Delta LWP/\Delta GMT$ ($\Delta IWP/\Delta GMT$) is a measure of the contribution of LWP (IWP) changes to the response of α to per degree warming ($\Delta\alpha/\Delta GMT$), which is proportional to their contributions to SW_{FB} (equation 1). Among the GCMs surveyed here, the median contribution to an α response from changes in LWP is inferred to be a factor of 14 larger than that arising from changes in IWP (Figure S10b). This result is consistent with the approximation in equation 1 that the SO SW_{FB} is dominated by LWP changes and the ability of equation 1 to predict the full radiative kernel calculation of SW_{FB} .

We combine our constraints on SW_{FB} for $40 - 50^\circ S$ and $50 - 85^\circ S$ to compute the constraint on $40 - 85^\circ S$ SW_{FB} . We take the sum of the area-weighted latitudinal constraints in $40 - 50^\circ S$ and $50 - 85^\circ S$ and propagate their standard errors to estimate $40 - 85^\circ S$ SW_{FB} . The contribution of the SO clouds to the global mean SW_{FB} is constrained to $-0.168 - 0.051 W m^{-2} K^{-1}$ with a 95% confidence interval (Figure 7). Considering potential systematic error in observations of LWP shifts the constraint on $40 - 85^\circ S$ SW_{FB} to $-0.192 - 0.047 W m^{-2} K^{-1}$. The constrained range of SO SW_{FB} is a bit wider than the range reported by McCoy et al. (2022), but we have added a new constraint from the $40 - 50^\circ S$ latitude band and have taken into account the uncertainty in radiative susceptibility arising from different α_{cs} thresholds and potential systematic uncertainties in observed LWP. Our constraint suggests that $40 - 85^\circ S$ SW_{FB} is less likely to be extremely negative or positive, as simulated by some CMIP6 GCMs. The most likely range of the SO SW_{FB} is from moderately negative to weakly positive.

4 Conclusions

In this work we built a CCF regression model to predict the response of the SO (40–85°S) LWP to global warming. The CCFs considered in the regression model were surface skin temperature, precipitation minus evaporation (approximately the moisture convergence), lower-tropospheric stability, and 500 mb subsidence. Warm and cold clouds are regulated by very different microphysical processes and have different responses to warming. To allow our CCF regression model to adapt to this, we partitioned the SO into cold and warm regimes. This new method increases the robustness of the CCF model prediction compared to previous work (McCoy et al., 2022). We used two out-of-sample tests to evaluate the predictive ability of our CCF regression model: the ability of our CCF model trained on observations to replicate the observed decadal trend in SO LWP (section 3.1.1; Figure 2) and the ability of our CCF model trained on the mean-state output of GCMs to predict their response to CO_2 quadrupling (section 3.1.2; Figure 3). Using the CCF regression model trained on observations combined with the GCM simulated changes in CCFs in response to CO_2 quadrupling, we were able to provide an observational constraint on the change in LWP in response to GMT ($\Delta LWP/\Delta GMT$) of $2.76 - 4.19 \text{ gm}^{-2}K^{-1}$ (Figure 3b).

Ultimately, the quantity we care about in relation to Earth’s radiation budget is not cloudiness, but radiative flux. We define a radiative susceptibility to liquid cloud ($\partial\alpha/\partial LWP$) that we can use to scale the LWP changes in response to warming. We compute $\partial\alpha/\partial LWP$ from satellite observations and GCM output. The observational constraint suggests that most of the GCMs overestimate $\partial\alpha/\partial LWP$ (Figure 5), which is consistent with recent studies of tropical clouds (Konsta et al., 2022). Satellite observations estimate $\partial\alpha/\partial LWP$ to be $0.43 - 0.90 \text{ (kg m}^{-2}\text{)}^{-1}$.

GCMs with higher mean-state LWP tend to have lower $\partial\alpha/\partial LWP$ (Figure 5)- resulting in compensation between macrophysical changes in cloud and radiative impact. This feature can be connected to the sensitivity of LWP to moisture convergence ($\partial LWP/\partial P - E$). GCMs with higher $\partial LWP/\partial P - E$ simulate higher mean-state LWP. These GCMs tend to predict a larger LWP response ($\Delta LWP/\Delta GMT$) but have a lower $\partial\alpha/\partial LWP$ due to radiative saturation.

Approximating SO SW_{FB} as the product of $\partial\alpha/\partial LWP$ and $\Delta LWP/\Delta GMT$ predicts roughly 50% of the variance in SO SW_{FB} across 50 CMIP5 and CMIP6 GCMs (Table S1) calculated from radiative kernels (Zelinka, Myers, McCoy, Po-Chedley, et al., 2020) (Figure 6). Observational constraints on $\Delta LWP/\Delta GMT$ and $\partial\alpha/\partial LWP$ produce a constrained range on SO SW_{FB} of -0.168 to $0.051 \text{ Wm}^{-2}K^{-1}$ (95% confidence interval) (Figure 7), which suggests a moderate negative to weakly positive SO SW_{FB} . This is consistent with previous work (McCoy et al., 2022), but expands the constraint region to the entire SO as opposed to just constraining the region where GCMs consistently moisten and more fully accounts for observational uncertainty.

Our analysis suggests some directions of future studies seeking to constrain extratropical SW_{FB} :

1. Our analysis identified increased moisture convergence into the SO as a key driver of increased LWP. This mechanism ultimately links the global circulation and hydrological cycle to the extratropical SW_{FB} . To better understand this linkage, it would be useful to understand how Hadley cell expansion and transient eddies (i.e. atmospheric rivers) contribute to long-term variability of the SO moisture budget.
2. Due to the lack of microwave observations of LWP over ice, we cannot provide an observationally-constrained CCF model for the cold regime. In this study, the GCM relationship between the warm regime LWP response and the response averaged over the latitude band including both cold and warm regimes provides an estimate

808 including uncertainty related to the cold regime. Ground-based LWP observations
 809 in high latitude SO, such as those taken during the Atmospheric Radiation Mea-
 810 surement (ARM) West Antarctic Radiation Experiment (AWARE, Lubin et al.
 811 (2020)), may be able to provide an observational constraint on the cold regime LWP
 812 response.

813 3. We found that $\partial\alpha/\partial LWP$ varied dramatically across GCMs and strongly mod-
 814 ulated the effect of changes in LWP on radiation. We also found that observations
 815 suggested that GCMs tended to have a $\partial\alpha/\partial LWP$ that was too large. One pos-
 816 sibility is that this is due to clouds that are too uniform and radiatively efficient
 817 (Konsta et al., 2022; Nam et al., 2012). Determining the origin of this behavior
 818 might be helpful in identifying a potential source of GCM bias in SW_{FB} .

819 5 Open Research

820 GCM outputs used in this study are available from Earth System Grid Federation
 821 (ESGF) esgf-node.llnl.gov (Cinquini et al., 2014)[Data]. The code for calculating the full
 822 shortwave cloud feedback data from GCM output is documented and published in (Zelinka,
 823 Myers, McCoy, Po-Chedley, et al., 2020) [Software] and at github.com/mzelinka. MAC-
 824 LWP and MERRA-2 reanalysis data are available from the Goddard Earth Sciences Data
 825 and Information Services Center at disc.gsfc.nasa.gov (Elsaesser et al., 2017a; Gelaro,
 826 McCarty, Suárez, et al., 2017) [Data]. CERES EBAF Edition 4.1 data is available from
 827 ceres.larc.nasa.gov (Loeb et al., 2018a) [Data].

828 Acknowledgments

829 The efforts of CT, DTM, and GSE are supported under NASA-PMMST Grant #80NSSC22K0599.
 830 GSE acknowledges additional support from the NASA Modeling, Analysis and Predic-
 831 tion Program and APAM GISS Co-Op #80NSSC18M0133. We thank Dr. Mark Zelinka
 832 for sharing his shortwave cloud feedback map data for all the GCMs included in this study.
 833 We appreciate the World Climate Research Programme (WCRP) for their promoting
 834 and coordinating efforts of CMIP. We also thank all modeling groups for producing and
 835 publishing their model output. We thank the Earth System Grid Federation (ESGF) for
 836 archiving and providing useful accessing tools to all model output, and the multiple fund-
 837 ing agencies that support CMIP5/6 and ESGF. We would like to acknowledge the use
 838 of computational resources (doi:10.5065/D6RX99HX) at the NCAR-Wyoming Super-
 839 computing Center provided by the National Science Foundation and the State of Wyoming,
 840 and supported by NCAR’s Computational and Information Systems Laboratory.

Relationships between SW_{FB} , LWP Response $\left(\frac{\Delta LWP}{\Delta GMT}\right)$, and Climate Sensitivity

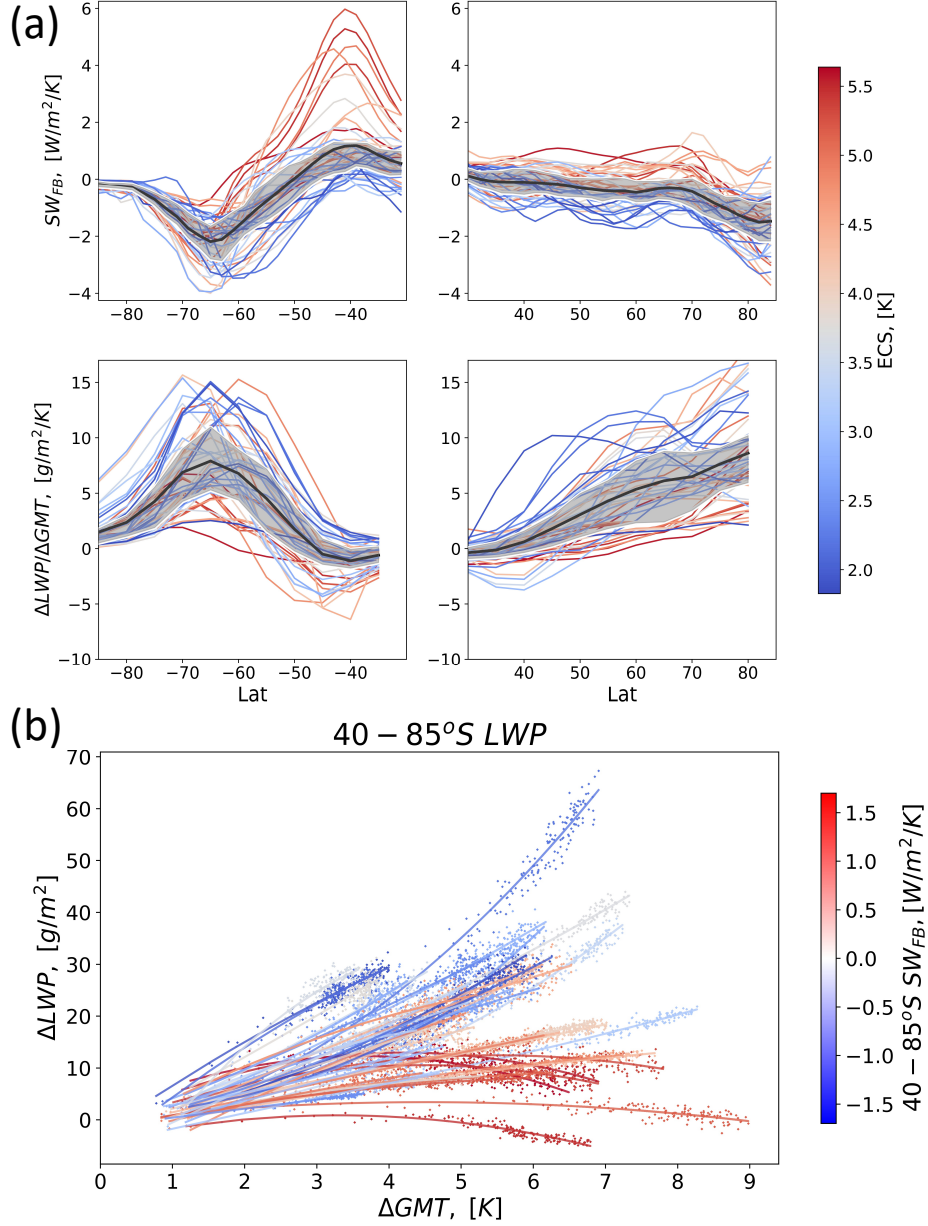


Figure 1. (a) Extratropical SW cloud feedback (SW_{FB}) (top) and the response of liquid water path (LWP) to global-mean temperature (GMT) ($\Delta LWP/\Delta GMT$) in the GCMs in Table S1. Anomalies in LWP and GMT are calculated as the differences between the mean of *piControl* and year 121 - 140's mean of *abrupt4xCO₂* simulations. Thick black lines are the multi-model mean and the shaded regions correspond to the 25th-75th percentiles of quantities. (b) Annual-mean anomalies in Southern Ocean (40 – 85°S) averaged LWP versus GMT relative to *piControl* average for the first 150 years of *abrupt4xCO₂* simulations. Lines show the second-order polynomial fit of the annual-mean LWP responses to GMT for each GCM. Lines for each GCM in (a) and (b) are colored by model effective climate sensitivity (ECS) and the 40 – 85° averaged SW_{FB} , respectively. SW_{FB} and effective climate sensitivity (ECS) data are from Zelinka, Myers, McCoy, Po-Chedley, et al. (2020).

Prediction of Observed LWP

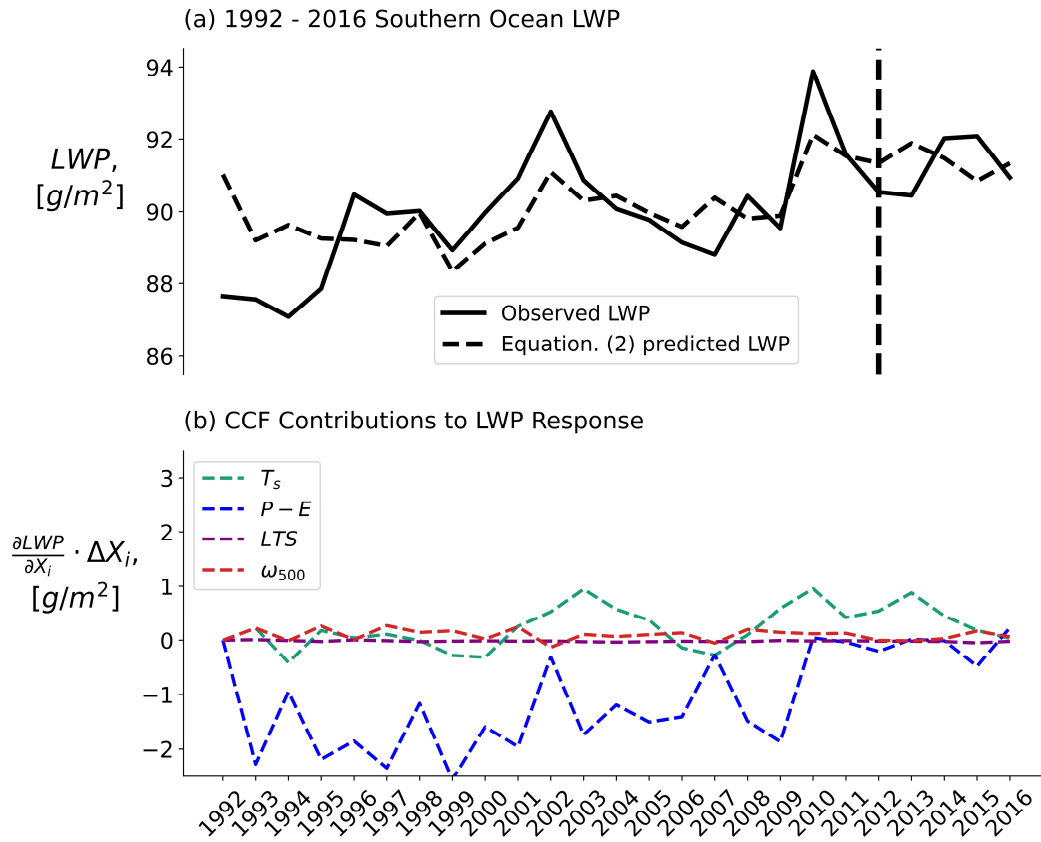


Figure 2. (a) Observed annual-mean Southern Ocean averaged LWP from MAC-LWP (green) and LWP predicted by the CCF model (Equation 2; blue) from 1992 to 2016. The CCF model is trained on monthly-mean data from 2012 to 2016 (right side of the dashed line) and is used to predict the annual-mean LWP back to 1992. (b) The decomposition of annual-mean LWP anomalies into individual CCF contributions by equation 2.

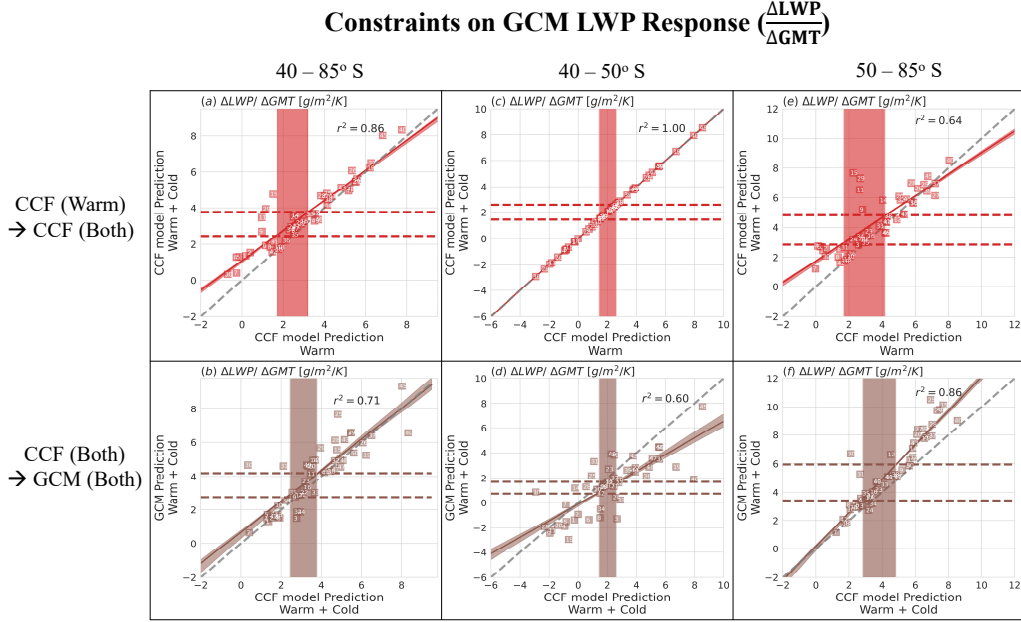


Figure 3. Predictions of the GCM-simulated LWP response to CO_2 quadrupling ($\Delta LWP/\Delta GMT$) by Equation 3. $\Delta LWP/\Delta GMT$ is shown averaged over (a,b) 40 – 85°S, (c,d) 40 – 50°S, and (e,f): 50 – 85°S. (a,c,e) Latitude-averaged $\Delta LWP/\Delta GMT$ predicted by equation 3 in warm and cold regimes versus only in the warm regime. (b,d,f) Latitude-averaged $\Delta LWP/\Delta GMT$ simulated by GCMs versus $\Delta LWP/\Delta GMT$ predicted by equation 3 in both regimes. 1-1 lines are shown using dashed gray lines and best-fit lines are shown as solid red and brown lines with their uncertainties estimated by Jackknife resampling. Observational constraints (red shading) are shown in (a,c,e). This constraint is propagated from the warm regime $\Delta LWP/\Delta GMT$ to the $\Delta LWP/\Delta GMT$ in both regimes by taking the intersection between the red shading and the best-fit line with its uncertainty (red dashed lines). Constraints on $\Delta LWP/\Delta GMT$ in both regimes are then shown in (b,d,f) using brown shading. The constrained ranges are combined with the uncertainty in the CCF model prediction by using the best-fit line between GCM and CCF model predictions to yield an observational constraint on GCM-simulated $\Delta LWP/\Delta GMT$ (brown dashed lines). Explained variance (r^2) is shown in each subplot. GCMs are denoted with the number listed in Table S1.

Decomposition on LWP Response ($\frac{\Delta LWP}{\Delta GMT}$)

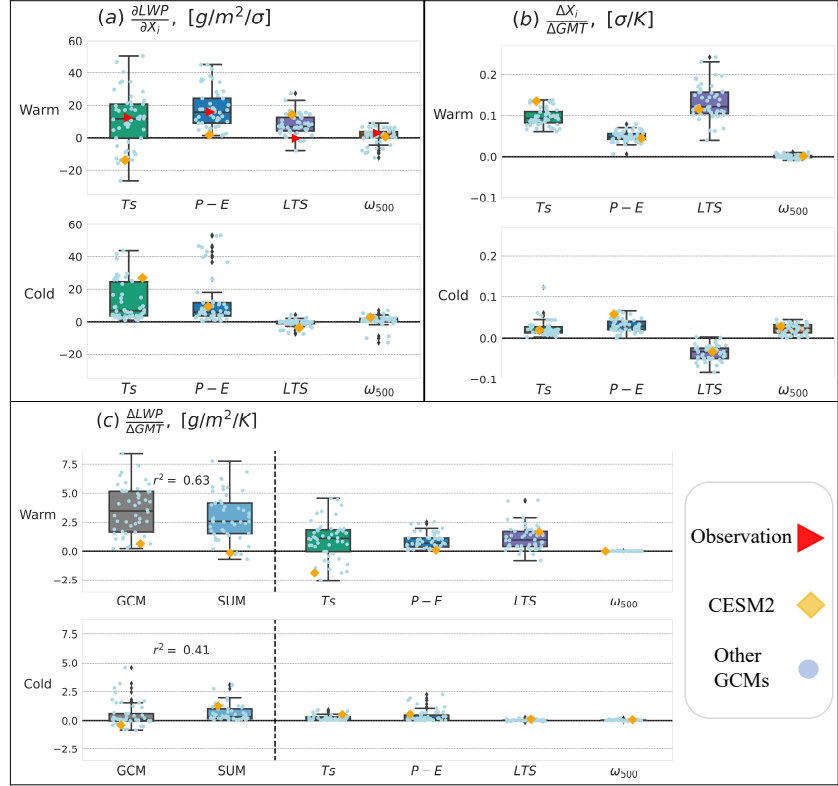


Figure 4. Decomposition of $\Delta LWP/\Delta GMT$ predicted by Equation 3: (a) Sensitivities of LWP each CCF; (b) standardized change in each CCF per degree warming; (c) LWP changes due to each CCF (the product of (a) with (b)), their sum (sky blue box), and the GCM-simulated LWP response (gray box). Cold and Warm regime values are shown separately. The variance (r^2) of GCM-simulated $\Delta LWP/\Delta GMT$ explained by the CCF model predictions in each regime is shown in subplot (c). Changes in CCFs are normalized by their spatio-temporal standard deviations of each regime in the mean-state climate. We single out one GCM, CESM2, by denoting its values as orange diamonds. All other GCMs are denoted as light blue dots. Observational sensitivities are denoted as red triangles in the warm regime.

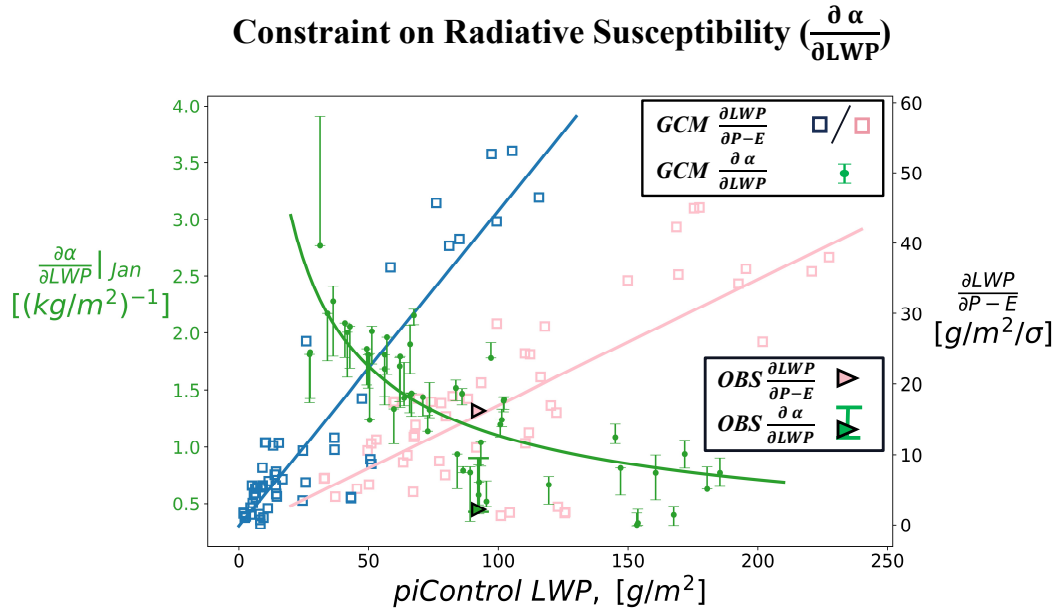


Figure 5. The radiative susceptibility ($\partial\alpha/\partial LWP$, left axis) and the sensitivity of LWP to moisture convergence ($\partial LWP/\partial P - E$, right axis) in the warm (pink) and cold (blue) regimes as a function of regime mean-state (*piControl*) LWP. Observed $\partial LWP/\partial P - E$ and $\partial\alpha/\partial LWP$ are shown by the pink and green triangles (observational $\partial LWP/\partial P - E$ is comparable to the warm regime values of GCMs for reason discussed in sections 2.1 and 2.2.3). The linear fit between $\partial LWP/\partial P - E$ and *piControl* LWP in each regime and the power law fit between $\partial\alpha/\partial LWP$ and *piControl* LWP are shown. Uncertainty in $\partial\alpha/\partial LWP$ from varying the maximum clear-sky albedo $TR_{\alpha_{cs}}$ from 0.11 to 0.30 is shown as an uncertainty range.

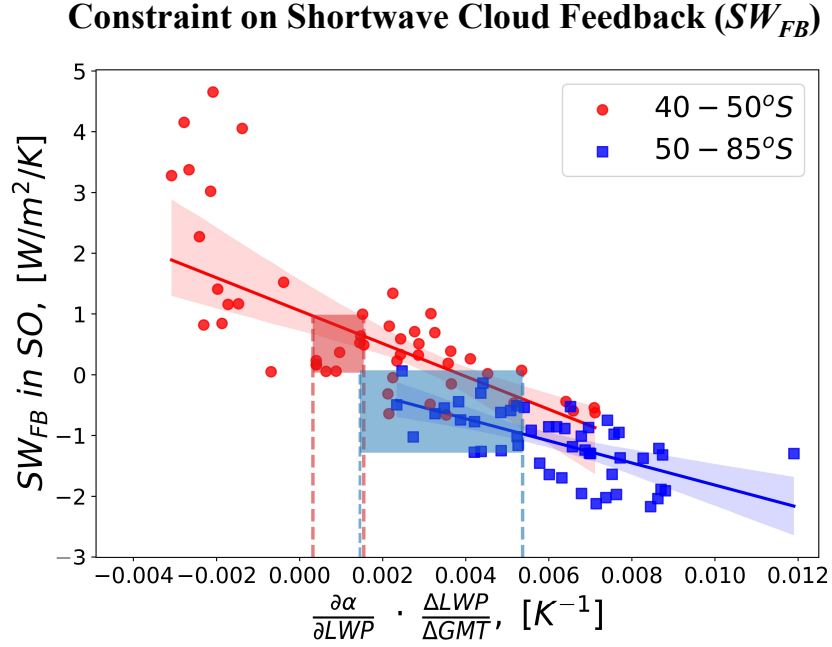


Figure 6. The SW cloud feedback of GCMs listed in Table S1 from Zelinka, Myers, McCoy, Po-Chedley, et al. (2020) for 40 – 50°S (red) and 50 – 85°S (blue) latitude bands versus predictions from the simplified physical model developed in this study (Equation 1). The observational constraints on 40 – 50°S and 50 – 85°S the constrained ranges on the y-axis of Figure 3 (d) and (f). The observational constraint on radiative susceptibilities ($\partial\alpha/\partial LWP$) is the error range of the green triangle in Figure 5. The combination of these two constraints yields constraints on 40 – 50°S and 50 – 85°S SW_{FB} , shown as shaded regions along the x-axis. Constrained 40 – 50°S and 50 – 85°S SW_{FB} are the extents of y-coordinate of models within the shaded regions. The linear fit between model SW_{FB} and predictions from equation 1 are shown with their 95% confidence interval.

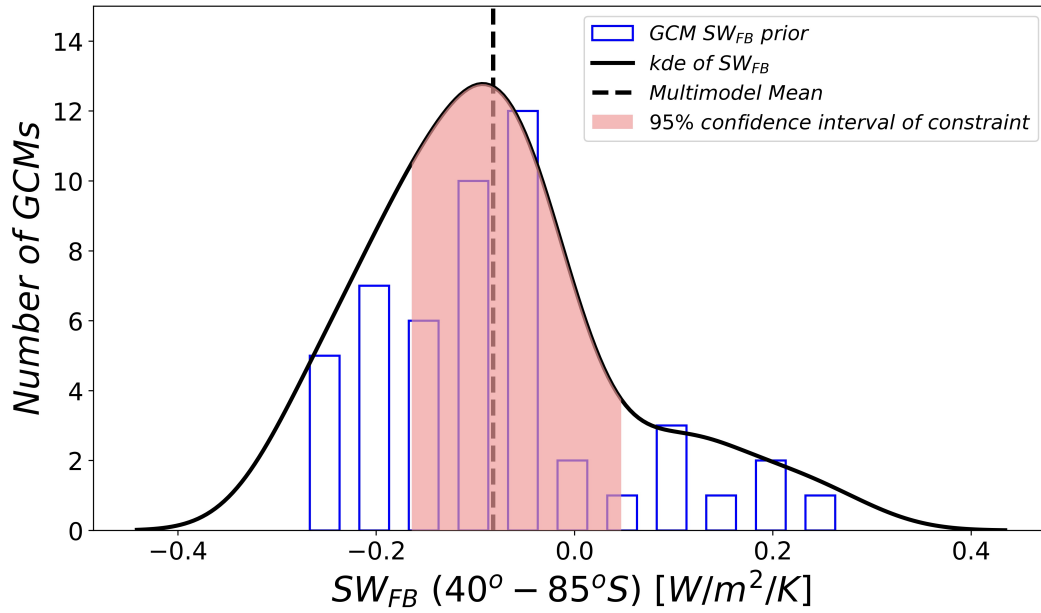


Figure 7. The contribution of Southern Ocean (40 – 85°S) SW_{FB} to the global mean cloud feedback. The prior distribution of SW_{FB} for GCMs listed in Table S1 is shown as the blue histograms and black kernel density estimate. The dashed black line denotes the multimodel mean of SW_{FB} for 50 GCMs. Red shading shows the 95% confidence interval of the Southern Ocean (40 – 85°S) averaged SW_{FB} by combining the constrained 40 – 50°S and 50 – 85°S averaged SW_{FB} shown in Figure 6. Observational constraint suggests a moderate negative to weak positive Southern Ocean SW_{FB} .

841

References

842

Allen, M. R., & Ingram, W. J. (2002, September). Constraints on future changes in climate and the hydrologic cycle. *Nature*, *419*(6903), 224–232. Retrieved 2023-02-27, from <https://www.nature.com/articles/nature01092> doi: 10.1038/nature01092

845

Andrews, T., Gregory, J. M., Webb, M. J., & Taylor, K. E. (2012, May). Forcing, feedbacks and climate sensitivity in CMIP5 coupled atmosphere-ocean climate models: CLIMATE SENSITIVITY IN CMIP5 MODELS. *Geophysical Research Letters*, *39*(9), n/a–n/a. Retrieved 2021-11-16, from <http://doi.wiley.com/10.1029/2012GL051607> doi: 10.1029/2012GL051607

849

Barnes, E. A., & Polvani, L. (2013, September). Response of the Midlatitude Jets, and of Their Variability, to Increased Greenhouse Gases in the CMIP5 Models. *Journal of Climate*, *26*(18), 7117–7135. Retrieved 2023-01-31, from <http://journals.ametsoc.org/doi/10.1175/JCLI-D-12-00536.1> doi: 10.1175/JCLI-D-12-00536.1

855

Bender, F. A.-M., Engström, A., Wood, R., & Charlson, R. J. (2017, June). Evaluation of Hemispheric Asymmetries in Marine Cloud Radiative Properties. *Journal of Climate*, *30*(11), 4131–4147. Retrieved 2022-06-14, from <http://journals.ametsoc.org/doi/10.1175/JCLI-D-16-0263.1> doi: 10.1175/JCLI-D-16-0263.1

860

Bender, F. A.-M., Ramanathan, V., & Tselioudis, G. (2012, May). Changes in extratropical storm track cloudiness 1983–2008: observational support for a poleward shift. *Climate Dynamics*, *38*(9-10), 2037–2053. Retrieved 2022-04-04, from <http://link.springer.com/10.1007/s00382-011-1065-6> doi: 10.1007/s00382-011-1065-6

865

Betts, A. K., & Harshvardhan. (1987). Thermodynamic constraint on the cloud liquid water feedback in climate models. *Journal of Geophysical Research*, *92*(D7), 8483. Retrieved 2022-05-20, from <http://doi.wiley.com/10.1029/JD092iD07p08483> doi: 10.1029/JD092iD07p08483

869

Bjordal, J., Storelvmo, T., Alterskjær, K., & Carlsen, T. (2020, November). Equilibrium climate sensitivity above 5 °C plausible due to state-dependent cloud feedback. *Nature Geoscience*, *13*(11), 718–721. Retrieved 2022-05-20, from <https://www.nature.com/articles/s41561-020-00649-1> doi: 10.1038/s41561-020-00649-1

874

Bodas-Salcedo, A., Webb, M. J., Bony, S., Chepfer, H., Dufresne, J.-L., Klein, S. A., ... John, V. O. (2011, August). COSP: Satellite simulation software for model assessment. *Bulletin of the American Meteorological Society*, *92*(8), 1023–1043. Retrieved 2022-05-20, from <https://journals.ametsoc.org/doi/10.1175/2011BAMS2856.1> doi: 10.1175/2011BAMS2856.1

879

Bodas-Salcedo, A., Mulcahy, J. P., Andrews, T., Williams, K. D., Ringer, M. A., Field, P. R., & Elsaesser, G. S. (2019, June). Strong Dependence of Atmospheric Feedbacks on Mixed-Phase Microphysics and Aerosol-Cloud Interactions in HadGEM3. *Journal of Advances in Modeling Earth Systems*, *11*(6), 1735–1758. Retrieved 2023-01-26, from <https://onlinelibrary.wiley.com/doi/10.1029/2019MS001688> doi: 10.1029/2019MS001688

885

Bonan, D. B., Siler, N., Roe, G. H., & Armour, K. C. (2023, February). Energetic constraints on the pattern of changes to the hydrological cycle under global warming. *Journal of Climate*, 1–48. Retrieved 2023-02-24, from <https://journals.ametsoc.org/view/journals/clim/aop/JCLI-D-22-0337.1/JCLI-D-22-0337.1.xml> doi: 10.1175/JCLI-D-22-0337.1

890

Bony, S., Colman, R., Kattsov, V. M., Allan, R. P., Bretherton, C. S., Dufresne, J.-L., ... Webb, M. J. (2006, August). How Well Do We Understand and Evaluate Climate Change Feedback Processes? *Journal of Climate*, *19*(15), 3445–3482. Retrieved 2023-08-17, from <http://journals.ametsoc.org/doi/10.1175/JCLI3819.1> doi: 10.1175/JCLI3819.1

895

- 896 Boucher, O., & el. (2014). *Climate Change 2013 – The Physical Science Basis:*
 897 *Working Group I Contribution to the Fifth Assessment Report of the Intergov-*
 898 *ernmental Panel on Climate Change* (1st ed.). Cambridge University Press.
 899 Retrieved 2023-08-24, from [https://www.cambridge.org/core/product/](https://www.cambridge.org/core/product/identifiner/9781107415324/type/book)
 900 [identifiner/9781107415324/type/book](https://www.cambridge.org/core/product/identifiner/9781107415324/type/book) doi: 10.1017/CBO9781107415324
- 901 Bretherton, C. S., Blossey, P. N., & Jones, C. R. (2013, June). Mechanisms of
 902 marine low cloud sensitivity to idealized climate perturbations: A single-
 903 LES exploration extending the CGILS cases. *Journal of Advances in*
 904 *Modeling Earth Systems*, 5(2), 316–337. Retrieved 2022-04-02, from
 905 <https://onlinelibrary.wiley.com/doi/10.1002/jame.20019> doi:
 906 10.1002/jame.20019
- 907 Bretherton, C. S., & Wyant, M. C. (1997, January). Moisture Transport, Lower-
 908 Tropospheric Stability, and Decoupling of Cloud-Topped Boundary Layers.
 909 *Journal of the Atmospheric Sciences*, 54(1), 148–167. Retrieved 2022-11-
 910 17, from [http://journals.ametsoc.org/doi/10.1175/1520-0469\(1997\)](http://journals.ametsoc.org/doi/10.1175/1520-0469(1997)054<0148:MTL TSA>2.0.CO;2)
 911 [054<0148:MTL TSA>2.0.CO;2](http://journals.ametsoc.org/doi/10.1175/1520-0469(1997)054<0148:MTL TSA>2.0.CO;2) doi: 10.1175/1520-0469(1997)054(0148:
 912 MTL TSA)2.0.CO;2
- 913 Brient, F., & Schneider, T. (2016, August). Constraints on Climate Sensitivity
 914 from Space-Based Measurements of Low-Cloud Reflection. *Journal of Climate*,
 915 29(16), 5821–5835. Retrieved 2023-01-22, from [http://journals.ametsoc](http://journals.ametsoc.org/doi/10.1175/JCLI-D-15-0897.1)
 916 [.org/doi/10.1175/JCLI-D-15-0897.1](http://journals.ametsoc.org/doi/10.1175/JCLI-D-15-0897.1) doi: 10.1175/JCLI-D-15-0897.1
- 917 Ceppi, P., Hartmann, D. L., & Webb, M. J. (2016, January). Mechanisms
 918 of the Negative Shortwave Cloud Feedback in Middle to High Lati-
 919 tudes. *Journal of Climate*, 29(1), 139–157. Retrieved 2023-02-22, from
 920 <http://journals.ametsoc.org/doi/10.1175/JCLI-D-15-0327.1> doi:
 921 10.1175/JCLI-D-15-0327.1
- 922 Ceppi, P., McCoy, D. T., & Hartmann, D. L. (2016, February). Observational ev-
 923 idence for a negative shortwave cloud feedback in middle to high latitudes.
 924 *Geophysical Research Letters*, 43(3), 1331–1339. Retrieved 2023-02-04, from
 925 <https://onlinelibrary.wiley.com/doi/10.1002/2015GL067499> doi:
 926 10.1002/2015GL067499
- 927 Cesana, G., Del Genio, A. D., Ackerman, A. S., Kelley, M., Elsaesser, G., Fridlind,
 928 A. M., ... Yao, M.-S. (2019, March). Evaluating models' response of
 929 tropical low clouds to SST forcings using CALIPSO observations. *Atmo-*
 930 *spheric Chemistry and Physics*, 19(5), 2813–2832. Retrieved 2022-04-
 931 03, from <https://acp.copernicus.org/articles/19/2813/2019/> doi:
 932 10.5194/acp-19-2813-2019
- 933 Cesana, G. V., & Del Genio, A. D. (2021, March). Observational constraint
 934 on cloud feedbacks suggests moderate climate sensitivity. *Nature Climate*
 935 *Change*, 11(3), 213–218. Retrieved 2022-04-08, from [http://www.nature.com/](http://www.nature.com/articles/s41558-020-00970-y)
 936 [articles/s41558-020-00970-y](http://www.nature.com/articles/s41558-020-00970-y) doi: 10.1038/s41558-020-00970-y
- 937 Cinquini, L., Crichton, D., Mattmann, C., Harney, J., Shipman, G., Wang, F., ...
 938 others (2014). *The earth system grid federation: An open infrastructure for*
 939 *access to distributed geospatial data* (Vol. 36) [dataset]. Elsevier.
- 940 Danabasoglu, G., Lamarque, J., Bacmeister, J., Bailey, D. A., DuVivier, A. K., Ed-
 941 wards, J., ... Strand, W. G. (2020, February). The Community Earth System
 942 Model Version 2 (CESM2). *Journal of Advances in Modeling Earth Systems*,
 943 12(2). Retrieved 2023-03-30, from [https://onlinelibrary.wiley.com/doi/](https://onlinelibrary.wiley.com/doi/10.1029/2019MS001916)
 944 [10.1029/2019MS001916](https://onlinelibrary.wiley.com/doi/10.1029/2019MS001916) doi: 10.1029/2019MS001916
- 945 Elsaesser, G. S., O'Dell, C. W., Lebsock, M. D., Bennartz, R., Greenwald, T. J., &
 946 Wentz, F. J. (2017a). *The multisensor advanced climatology of liquid water*
 947 *path (mac-lwp)* (Vol. 30) (dataset No. 24). American Meteorological Society.
- 948 Elsaesser, G. S., O'Dell, C. W., Lebsock, M. D., Bennartz, R., Greenwald, T. J., &
 949 Wentz, F. J. (2017b, December). The Multisensor Advanced Climatology of
 950 Liquid Water Path (MAC-LWP). *Journal of Climate*, 30(24), 10193–10210.

- 951 Retrieved 2022-09-06, from [https://journals.ametsoc.org/doi/10.1175/
952 JCLI-D-16-0902.1](https://journals.ametsoc.org/doi/10.1175/JCLI-D-16-0902.1) doi: 10.1175/JCLI-D-16-0902.1
- 953 Field, P. R., & Heymsfield, A. J. (2015, November). Importance of snow to
954 global precipitation. *Geophysical Research Letters*, *42*(21), 9512–9520. Re-
955 trieved 2023-03-22, from [https://onlinelibrary.wiley.com/doi/10.1002/
956 2015GL065497](https://onlinelibrary.wiley.com/doi/10.1002/2015GL065497) doi: 10.1002/2015GL065497
- 957 Field, P. R., & Wood, R. (2007, January). Precipitation and Cloud Structure in
958 Midlatitude Cyclones. *Journal of Climate*, *20*(2), 233–254. Retrieved 2023-10-
959 18, from <http://journals.ametsoc.org/doi/10.1175/JCLI3998.1> doi: 10
960 .1175/JCLI3998.1
- 961 Forster, P., & el. (2023). *Climate Change 2021 – The Physical Science Basis:
962 Working Group I Contribution to the Sixth Assessment Report of the Intergov-
963 ernmental Panel on Climate Change* (1st ed.). Cambridge University Press.
964 Retrieved 2023-08-23, from [https://www.cambridge.org/core/product/
965 identifier/9781009157896/type/book](https://www.cambridge.org/core/product/identifier/9781009157896/type/book) doi: 10.1017/9781009157896.009
- 966 Frazer, M. E., & Ming, Y. (2022, April). Understanding the Extratropical Liq-
967 uid Water Path Feedback in Mixed-Phase Clouds with an Idealized Global
968 Climate Model. *Journal of Climate*, *35*(8), 2391–2406. Retrieved 2023-
969 01-26, from [https://journals.ametsoc.org/view/journals/clim/35/8/
970 JCLI-D-21-0334.1.xml](https://journals.ametsoc.org/view/journals/clim/35/8/JCLI-D-21-0334.1.xml) doi: 10.1175/JCLI-D-21-0334.1
- 971 Frey, W. R., & Kay, J. E. (2018, April). The influence of extratropical cloud phase
972 and amount feedbacks on climate sensitivity. *Climate Dynamics*, *50*(7-8),
973 3097–3116. Retrieved 2023-07-05, from [http://link.springer.com/10.1007/
974 s00382-017-3796-5](http://link.springer.com/10.1007/s00382-017-3796-5) doi: 10.1007/s00382-017-3796-5
- 975 Gelaro, R., McCarty, W., Suárez, M. J., Todling, R., Molod, A., Takacs, L., ... oth-
976 ers (2017). *The modern-era retrospective analysis for research and applications,
977 version 2 (merra-2)* (Vol. 30) (dataset No. 14).
- 978 Gelaro, R., McCarty, W., Suárez, M. J., Todling, R., Molod, A., Takacs, L., ...
979 Zhao, B. (2017, July). The Modern-Era Retrospective Analysis for Research
980 and Applications, Version 2 (MERRA-2). *Journal of Climate*, *30*(14), 5419–
981 5454. Retrieved 2023-03-29, from [https://journals.ametsoc.org/doi/
982 10.1175/JCLI-D-16-0758.1](https://journals.ametsoc.org/doi/10.1175/JCLI-D-16-0758.1) doi: 10.1175/JCLI-D-16-0758.1
- 983 Gettelman, A., Hannay, C., Bacmeister, J. T., Neale, R. B., Pendergrass, A. G.,
984 Danabasoglu, G., ... Mills, M. J. (2019, July). High Climate Sensitiv-
985 ity in the Community Earth System Model Version 2 (CESM2). *Geo-
986 physical Research Letters*, *46*(14), 8329–8337. Retrieved 2023-02-02, from
987 <https://onlinelibrary.wiley.com/doi/10.1029/2019GL083978> doi:
988 10.1029/2019GL083978
- 989 Golaz, J., Caldwell, P. M., Van Roekel, L. P., Petersen, M. R., Tang, Q., Wolfe,
990 J. D., ... Zhu, Q. (2019, July). The DOE E3SM Coupled Model Version
991 1: Overview and Evaluation at Standard Resolution. *Journal of Advances
992 in Modeling Earth Systems*, *11*(7), 2089–2129. Retrieved 2023-08-17, from
993 <https://onlinelibrary.wiley.com/doi/abs/10.1029/2018MS001603> doi:
994 10.1029/2018MS001603
- 995 Gordon, N. D., & Klein, S. A. (2014, May). Low-cloud optical depth feedback
996 in climate models: Optical Depth Feedback. *Journal of Geophysical Re-
997 search: Atmospheres*, *119*(10), 6052–6065. Retrieved 2022-03-29, from [http://
998 doi.wiley.com/10.1002/2013JD021052](http://doi.wiley.com/10.1002/2013JD021052) doi: 10.1002/2013JD021052
- 999 Greenwald, T. J., Bennartz, R., Lebsock, M., & Teixeira, J. (2018, April). An Uncer-
1000 tainty Data Set for Passive Microwave Satellite Observations of Warm Cloud
1001 Liquid Water Path. *Journal of Geophysical Research: Atmospheres*, *123*(7),
1002 3668–3687. Retrieved 2023-06-23, from [https://onlinelibrary.wiley.com/
1003 doi/10.1002/2017JD027638](https://onlinelibrary.wiley.com/doi/10.1002/2017JD027638) doi: 10.1002/2017JD027638
- 1004 Grise, K. M., & Medeiros, B. (2016, December). Understanding the Varied Influence
1005 of Midlatitude Jet Position on Clouds and Cloud Radiative Effects in Obser-

- 1006 variations and Global Climate Models. *Journal of Climate*, 29(24), 9005–9025.
 1007 Retrieved 2022-04-03, from [http://journals.ametsoc.org/doi/10.1175/](http://journals.ametsoc.org/doi/10.1175/JCLI-D-16-0295.1)
 1008 [JCLI-D-16-0295.1](http://journals.ametsoc.org/doi/10.1175/JCLI-D-16-0295.1) doi: 10.1175/JCLI-D-16-0295.1
- 1009 Haynes, J. M., Jakob, C., Rossow, W. B., Tselioudis, G., & Brown, J. (2011, Oc-
 1010 tober). Major Characteristics of Southern Ocean Cloud Regimes and Their
 1011 Effects on the Energy Budget. *Journal of Climate*, 24(19), 5061–5080. Re-
 1012 trieved 2022-04-03, from [https://journals.ametsoc.org/doi/10.1175/](https://journals.ametsoc.org/doi/10.1175/2011JCLI4052.1)
 1013 [2011JCLI4052.1](https://journals.ametsoc.org/doi/10.1175/2011JCLI4052.1) doi: 10.1175/2011JCLI4052.1
- 1014 Held, I. M., & Soden, B. J. (2006, November). Robust Responses of the Hydrological
 1015 Cycle to Global Warming. *Journal of Climate*, 19(21), 5686–5699. Retrieved
 1016 2022-09-02, from <http://journals.ametsoc.org/doi/10.1175/JCLI3990.1>
 1017 doi: 10.1175/JCLI3990.1
- 1018 Houghton, J. T., & el. (2001). *Climate change 2001: the scientific basis: contribu-*
 1019 *tion of Working Group I to the third assessment report of the Intergovernmen-*
 1020 *tal Panel on Climate Change.* Cambridge ; New York: Cambridge University
 1021 Press.
- 1022 Huang, Y., Xia, Y., & Tan, X. (2017, October). On the pattern of CO₂ radia-
 1023 tive forcing and poleward energy transport: CO₂ Forcing Pattern and En-
 1024 ergy Transport. *Journal of Geophysical Research: Atmospheres*, 122(20),
 1025 10,578–10,593. Retrieved 2023-07-13, from [http://doi.wiley.com/10.1002/](http://doi.wiley.com/10.1002/2017JD027221)
 1026 [2017JD027221](http://doi.wiley.com/10.1002/2017JD027221) doi: 10.1002/2017JD027221
- 1027 Jiang, J. H., Su, H., Zhai, C., Perun, V. S., Del Genio, A., Nazarenko, L. S., ...
 1028 Stephens, G. L. (2012, July). Evaluation of cloud and water vapor sim-
 1029 ulations in CMIP5 climate models using NASA “A-Train” satellite obser-
 1030 vations: EVALUATION OF IPCC AR5 MODEL SIMULATIONS. *Jour-*
 1031 *nal of Geophysical Research: Atmospheres*, 117(D14), n/a–n/a. Retrieved
 1032 2023-02-03, from <http://doi.wiley.com/10.1029/2011JD017237> doi:
 1033 [10.1029/2011JD017237](http://doi.wiley.com/10.1029/2011JD017237)
- 1034 Klein, S. A., Hall, A., Norris, J. R., & Pincus, R. (2017, November). Low-Cloud
 1035 Feedbacks from Cloud-Controlling Factors: A Review. *Surveys in Geophysics*,
 1036 38(6), 1307–1329. Retrieved 2021-06-21, from [http://link.springer.com/10](http://link.springer.com/10.1007/s10712-017-9433-3)
 1037 [.1007/s10712-017-9433-3](http://link.springer.com/10.1007/s10712-017-9433-3) doi: 10.1007/s10712-017-9433-3
- 1038 Klein, S. A., & Hartmann, D. L. (1993, August). The Seasonal Cycle of Low Strati-
 1039 form Clouds. *Journal of Climate*, 6(8), 1587–1606. Retrieved 2023-03-12, from
 1040 [http://journals.ametsoc.org/doi/10.1175/1520-0442\(1993\)006<1587:](http://journals.ametsoc.org/doi/10.1175/1520-0442(1993)006<1587:TSCOLS>2.0.CO;2)
 1041 [TSCOLS>2.0.CO;2](http://journals.ametsoc.org/doi/10.1175/1520-0442(1993)006(1587:TSCOLS)2.0.CO;2) doi: 10.1175/1520-0442(1993)006(1587:TSCOLS)2.0.CO;2
- 1042 Komurcu, M., Storelvmo, T., Tan, I., Lohmann, U., Yun, Y., Penner, J. E., ...
 1043 Takemura, T. (2014, March). Intercomparison of the cloud water phase
 1044 among global climate models: CLOUD WATER PHASE IN GCMs. *Jour-*
 1045 *nal of Geophysical Research: Atmospheres*, 119(6), 3372–3400. Retrieved
 1046 2023-03-23, from <http://doi.wiley.com/10.1002/2013JD021119> doi:
 1047 [10.1002/2013JD021119](http://doi.wiley.com/10.1002/2013JD021119)
- 1048 Konsta, D., Dufresne, J., Chepfer, H., Vial, J., Koshiro, T., Kawai, H., ... Ogura,
 1049 T. (2022, June). Low-Level Marine Tropical Clouds in Six CMIP6 Mod-
 1050 els Are Too Few, Too Bright but Also Too Compact and Too Homoge-
 1051 neous. *Geophysical Research Letters*, 49(11). Retrieved 2023-03-30, from
 1052 <https://onlinelibrary.wiley.com/doi/10.1029/2021GL097593> doi:
 1053 [10.1029/2021GL097593](https://onlinelibrary.wiley.com/doi/10.1029/2021GL097593)
- 1054 Lacis, A. A., & Hansen, J. (1974, January). A Parameterization for the Absorption
 1055 of Solar Radiation in the Earth’s Atmosphere. *Journal of the Atmospheric Sci-*
 1056 *ences*, 31(1), 118–133. Retrieved 2023-03-30, from [http://journals.ametsoc](http://journals.ametsoc.org/doi/10.1175/1520-0469(1974)031<0118:APFTAO>2.0.CO;2)
 1057 [.org/doi/10.1175/1520-0469\(1974\)031<0118:APFTAO>2.0.CO;2](http://journals.ametsoc.org/doi/10.1175/1520-0469(1974)031<0118:APFTAO>2.0.CO;2) doi:
 1058 [10.1175/1520-0469\(1974\)031\(0118:APFTAO\)2.0.CO;2](http://journals.ametsoc.org/doi/10.1175/1520-0469(1974)031(0118:APFTAO)2.0.CO;2)
- 1059 Liou, K.-N. (2002). *An introduction to atmospheric radiation* (2nd ed ed.). Amster-
 1060 dam: Academic Press. (OCLC: 156781712)

- 1061 Loeb, N. G., Doelling, D. R., Wang, H., Su, W., Nguyen, C., Corbett, J. G., ...
 1062 Kato, S. (2018a). *Clouds and the earth's radiant energy system (ceres) en-*
 1063 *ergy balanced and filled (ebaf) top-of-atmosphere (toa) edition-4.0 data product*
 1064 (Vol. 31) (dataset No. 2).
- 1065 Loeb, N. G., Doelling, D. R., Wang, H., Su, W., Nguyen, C., Corbett, J. G., ...
 1066 Kato, S. (2018b, January). Clouds and the Earth's Radiant Energy Sys-
 1067 tem (CERES) Energy Balanced and Filled (EBAF) Top-of-Atmosphere
 1068 (TOA) Edition-4.0 Data Product. *Journal of Climate*, *31*(2), 895–918. Re-
 1069 trieved 2023-01-19, from [https://journals.ametsoc.org/doi/10.1175/](https://journals.ametsoc.org/doi/10.1175/JCLI-D-17-0208.1)
 1070 [JCLI-D-17-0208.1](https://journals.ametsoc.org/doi/10.1175/JCLI-D-17-0208.1) doi: 10.1175/JCLI-D-17-0208.1
- 1071 Loeb, N. G., Rose, F. G., Kato, S., Rutan, D. A., Su, W., Wang, H., ... Gettel-
 1072 man, A. (2020, January). Toward a Consistent Definition between Satellite
 1073 and Model Clear-Sky Radiative Fluxes. *Journal of Climate*, *33*(1), 61–75.
 1074 Retrieved 2023-08-09, from [http://journals.ametsoc.org/doi/10.1175/](http://journals.ametsoc.org/doi/10.1175/JCLI-D-19-0381.1)
 1075 [JCLI-D-19-0381.1](http://journals.ametsoc.org/doi/10.1175/JCLI-D-19-0381.1) doi: 10.1175/JCLI-D-19-0381.1
- 1076 Lorenz, D. J., & DeWeaver, E. T. (2007, July). The Response of the Extratrop-
 1077 ical Hydrological Cycle to Global Warming. *Journal of Climate*, *20*(14),
 1078 3470–3484. Retrieved 2023-04-19, from [http://journals.ametsoc.org/doi/](http://journals.ametsoc.org/doi/10.1175/JCLI4192.1)
 1079 [10.1175/JCLI4192.1](http://journals.ametsoc.org/doi/10.1175/JCLI4192.1) doi: 10.1175/JCLI4192.1
- 1080 Lubin, D., Zhang, D., Silber, I., Scott, R. C., Kalogeras, P., Battaglia, A., ... Vogel-
 1081 mann, A. M. (2020, July). AWARE: The Atmospheric Radiation Measurement
 1082 (ARM) West Antarctic Radiation Experiment. *Bulletin of the American Mete-*
 1083 *orological Society*, *101*(7), E1069–E1091. Retrieved 2023-04-13, from [https://](https://journals.ametsoc.org/view/journals/bams/101/7/bamsD180278.xml)
 1084 journals.ametsoc.org/view/journals/bams/101/7/bamsD180278.xml doi:
 1085 10.1175/BAMS-D-18-0278.1
- 1086 Manaster, A., O'Dell, C. W., & Elsaesser, G. (2017, August). Evaluation of Cloud
 1087 Liquid Water Path Trends Using a Multidecadal Record of Passive Microwave
 1088 Observations. *Journal of Climate*, *30*(15), 5871–5884. Retrieved 2023-01-24,
 1089 from <https://journals.ametsoc.org/doi/10.1175/JCLI-D-16-0399.1> doi:
 1090 10.1175/JCLI-D-16-0399.1
- 1091 Marchand, R., Haynes, J., Mace, G. G., Ackerman, T., & Stephens, G. (2009,
 1092 January). A comparison of simulated cloud radar output from the multi-
 1093 scale modeling framework global climate model with CloudSat cloud radar
 1094 observations. *Journal of Geophysical Research*, *114*, D00A20. Retrieved
 1095 2023-08-24, from <http://doi.wiley.com/10.1029/2008JD009790> doi:
 1096 10.1029/2008JD009790
- 1097 McCoy, D. T., Eastman, R., Hartmann, D. L., & Wood, R. (2017, May). The
 1098 Change in Low Cloud Cover in a Warmed Climate Inferred from AIRS,
 1099 MODIS, and ERA-Interim. *Journal of Climate*, *30*(10), 3609–3620. Re-
 1100 trieved 2022-03-27, from [http://journals.ametsoc.org/doi/10.1175/](http://journals.ametsoc.org/doi/10.1175/JCLI-D-15-0734.1)
 1101 [JCLI-D-15-0734.1](http://journals.ametsoc.org/doi/10.1175/JCLI-D-15-0734.1) doi: 10.1175/JCLI-D-15-0734.1
- 1102 McCoy, D. T., Field, P., Bodas-Salcedo, A., Elsaesser, G. S., & Zelinka, M. D. (2020,
 1103 December). A Regime-Oriented Approach to Observationally Constraining
 1104 Extratropical Shortwave Cloud Feedbacks. *Journal of Climate*, *33*(23),
 1105 9967–9983. Retrieved 2020-11-29, from [https://journals.ametsoc.org/](https://journals.ametsoc.org/jcli/article/33/23/9967/354498/A-Regime-Oriented-Approach-to-Observationally)
 1106 [jcli/article/33/23/9967/354498/A-Regime-Oriented-Approach-to-](https://journals.ametsoc.org/jcli/article/33/23/9967/354498/A-Regime-Oriented-Approach-to-Observationally)
 1107 [-Observationally](https://journals.ametsoc.org/jcli/article/33/23/9967/354498/A-Regime-Oriented-Approach-to-Observationally) (Publisher: American Meteorological Society) doi:
 1108 10.1175/JCLI-D-19-0987.1
- 1109 McCoy, D. T., Field, P., Frazer, M. E., Zelinka, M. D., Elsaesser, G. S.,
 1110 Mühlentstädt, J., ... Lebo, Z. J. (2022, April). Extratropical Shortwave
 1111 Cloud Feedbacks in the Context of the Global Circulation and Hydrologi-
 1112 cal Cycle. *Geophysical Research Letters*, *49*(8). Retrieved 2022-09-13, from
 1113 <https://onlinelibrary.wiley.com/doi/10.1029/2021GL097154> doi:
 1114 10.1029/2021GL097154
- 1115 McCoy, D. T., Field, P., Gordon, H., Elsaesser, G. S., & Grosvenor, D. P. (2020,

- 1116 April). Untangling causality in midlatitude aerosol–cloud adjustments. *At-*
 1117 *mospheric Chemistry and Physics*, 20(7), 4085–4103. Retrieved 2023-04-
 1118 13, from <https://acp.copernicus.org/articles/20/4085/2020/> doi:
 1119 10.5194/acp-20-4085-2020
- 1120 McCoy, D. T., Field, P. R., Elsaesser, G. S., Bodas-Salcedo, A., Kahn, B. H.,
 1121 Zelinka, M. D., ... Wilkinson, J. (2019, January). Cloud feedbacks in ex-
 1122 tratropical cyclones: insight from long-term satellite data and high-resolution
 1123 global simulations. *Atmospheric Chemistry and Physics*, 19(2), 1147–1172. Re-
 1124 trieved 2022-09-02, from [https://acp.copernicus.org/articles/19/1147/](https://acp.copernicus.org/articles/19/1147/2019/)
 1125 2019/ doi: 10.5194/acp-19-1147-2019
- 1126 McCoy, D. T., Field, P. R., Schmidt, A., Grosvenor, D. P., Bender, F. A.-M.,
 1127 Shipway, B. J., ... Elsaesser, G. S. (2018, April). Aerosol midlatitude cy-
 1128 clone indirect effects in observations and high-resolution simulations. *At-*
 1129 *mospheric Chemistry and Physics*, 18(8), 5821–5846. Retrieved 2022-05-
 1130 20, from <https://acp.copernicus.org/articles/18/5821/2018/> doi:
 1131 10.5194/acp-18-5821-2018
- 1132 McCoy, D. T., Hartmann, D. L., & Grosvenor, D. P. (2014, December). Observed
 1133 Southern Ocean Cloud Properties and Shortwave Reflection. Part II: Phase
 1134 Changes and Low Cloud Feedback*. *Journal of Climate*, 27(23), 8858–8868.
 1135 Retrieved 2022-12-21, from [http://journals.ametsoc.org/doi/10.1175/](http://journals.ametsoc.org/doi/10.1175/JCLI-D-14-00288.1)
 1136 JCLI-D-14-00288.1 doi: 10.1175/JCLI-D-14-00288.1
- 1137 McCoy, D. T., Tan, I., Hartmann, D. L., Zelinka, M. D., & Storelmo, T. (2016,
 1138 June). On the relationships among cloud cover, mixed-phase partitioning, and
 1139 planetary albedo in GCMs. *Journal of Advances in Modeling Earth Systems*,
 1140 8(2), 650–668. Retrieved 2022-06-14, from [https://onlinelibrary.wiley](https://onlinelibrary.wiley.com/doi/10.1002/2015MS000589)
 1141 [.com/doi/10.1002/2015MS000589](https://onlinelibrary.wiley.com/doi/10.1002/2015MS000589) doi: 10.1002/2015MS000589
- 1142 Morrison, H., de Boer, G., Feingold, G., Harrington, J., Shupe, M. D., & Su-
 1143 lia, K. (2012, January). Resilience of persistent Arctic mixed-phase
 1144 clouds. *Nature Geoscience*, 5(1), 11–17. Retrieved 2023-02-07, from
 1145 <http://www.nature.com/articles/ngeo1332> doi: 10.1038/ngeo1332
- 1146 Myers, T. A., & Norris, J. R. (2013, October). Observational Evidence That
 1147 Enhanced Subsidence Reduces Subtropical Marine Boundary Layer Cloudi-
 1148 ness. *Journal of Climate*, 26(19), 7507–7524. Retrieved 2021-12-06, from
 1149 <http://journals.ametsoc.org/doi/10.1175/JCLI-D-12-00736.1> doi:
 1150 10.1175/JCLI-D-12-00736.1
- 1151 Myers, T. A., & Norris, J. R. (2015, April). On the Relationships between Sub-
 1152 tropical Clouds and Meteorology in Observations and CMIP3 and CMIP5
 1153 Models*. *Journal of Climate*, 28(8), 2945–2967. Retrieved 2023-04-13, from
 1154 <http://journals.ametsoc.org/doi/10.1175/JCLI-D-14-00475.1> doi:
 1155 10.1175/JCLI-D-14-00475.1
- 1156 Myers, T. A., & Norris, J. R. (2016, March). Reducing the uncertainty in sub-
 1157 tropical cloud feedback. *Geophysical Research Letters*, 43(5), 2144–2148. Re-
 1158 trieved 2021-12-06, from [https://onlinelibrary.wiley.com/doi/10.1002/](https://onlinelibrary.wiley.com/doi/10.1002/2015GL067416)
 1159 2015GL067416 doi: 10.1002/2015GL067416
- 1160 Myers, T. A., Scott, R. C., Zelinka, M. D., Klein, S. A., Norris, J. R., & Cald-
 1161 well, P. M. (2021, June). Observational constraints on low cloud feedback
 1162 reduce uncertainty of climate sensitivity. *Nature Climate Change*, 11(6),
 1163 501–507. Retrieved 2021-06-21, from [http://www.nature.com/articles/](http://www.nature.com/articles/s41558-021-01039-0)
 1164 s41558-021-01039-0 doi: 10.1038/s41558-021-01039-0
- 1165 Nam, C., Bony, S., Dufresne, J.-L., & Chepfer, H. (2012, November). The ‘too few,
 1166 too bright’ tropical low-cloud problem in CMIP5 models: TOO FEW TOO
 1167 BRIGHT LOW-CLOUDS. *Geophysical Research Letters*, 39(21), n/a–n/a.
 1168 Retrieved 2023-03-30, from <http://doi.wiley.com/10.1029/2012GL053421>
 1169 doi: 10.1029/2012GL053421
- 1170 Norris, J. R., Allen, R. J., Evan, A. T., Zelinka, M. D., O’Dell, C. W., & Klein,

- 1171 S. A. (2016, August). Evidence for climate change in the satellite cloud
1172 record. *Nature*, *536*(7614), 72–75. Retrieved 2023-08-23, from [https://](https://www.nature.com/articles/nature18273)
1173 www.nature.com/articles/nature18273 doi: 10.1038/nature18273
- 1174 Qu, X., Hall, A., Klein, S. A., & DeAngelis, A. M. (2015, September). Positive
1175 tropical marine low-cloud cover feedback inferred from cloud-controlling fac-
1176 tors. *Geophysical Research Letters*, *42*(18), 7767–7775. Retrieved 2021-03-28,
1177 from <https://onlinelibrary.wiley.com/doi/10.1002/2015GL065627> doi:
1178 10.1002/2015GL065627
- 1179 Rasch, P. J., Xie, S., Ma, P., Lin, W., Wang, H., Tang, Q., ... Yang, Y. (2019,
1180 August). An Overview of the Atmospheric Component of the Energy Exascale
1181 Earth System Model. *Journal of Advances in Modeling Earth Systems*, *11*(8),
1182 2377–2411. Retrieved 2023-08-17, from [https://onlinelibrary.wiley.com/](https://onlinelibrary.wiley.com/doi/10.1029/2019MS001629)
1183 [doi/10.1029/2019MS001629](https://onlinelibrary.wiley.com/doi/10.1029/2019MS001629) doi: 10.1029/2019MS001629
- 1184 Rieck, M., Nuijens, L., & Stevens, B. (2012, August). Marine Boundary Layer
1185 Cloud Feedbacks in a Constant Relative Humidity Atmosphere. *Journal of*
1186 *the Atmospheric Sciences*, *69*(8), 2538–2550. Retrieved 2022-04-03, from
1187 <https://journals.ametsoc.org/doi/10.1175/JAS-D-11-0203.1> doi:
1188 10.1175/JAS-D-11-0203.1
- 1189 Scott, R. C., Myers, T. A., Norris, J. R., Zelinka, M. D., Klein, S. A., Sun, M.,
1190 & Doelling, D. R. (2020, September). Observed Sensitivity of Low-Cloud
1191 Radiative Effects to Meteorological Perturbations over the Global Oceans.
1192 *Journal of Climate*, *33*(18), 7717–7734. Retrieved 2022-07-28, from [https://](https://journals.ametsoc.org/view/journals/clim/33/18/jcliD191028.xml)
1193 journals.ametsoc.org/view/journals/clim/33/18/jcliD191028.xml doi:
1194 10.1175/JCLI-D-19-1028.1
- 1195 Seager, R., & Henderson, N. (2013, October). Diagnostic Computation of Moisture
1196 Budgets in the ERA-Interim Reanalysis with Reference to Analysis of CMIP-
1197 Archived Atmospheric Model Data*. *Journal of Climate*, *26*(20), 7876–7901.
1198 Retrieved 2021-03-28, from [http://journals.ametsoc.org/doi/10.1175/](http://journals.ametsoc.org/doi/10.1175/JCLI-D-13-00018.1)
1199 [JCLI-D-13-00018.1](http://journals.ametsoc.org/doi/10.1175/JCLI-D-13-00018.1) doi: 10.1175/JCLI-D-13-00018.1
- 1200 Senior, C. A., & Mitchell, J. F. B. (1993, March). Carbon Dioxide and Cli-
1201 mate. The Impact of Cloud Parameterization. *Journal of Climate*, *6*(3),
1202 393–418. Retrieved 2023-02-22, from [http://journals.ametsoc.org/](http://journals.ametsoc.org/doi/10.1175/1520-0442(1993)006<0393:CDACTI>2.0.CO;2)
1203 [doi/10.1175/1520-0442\(1993\)006<0393:CDACTI>2.0.CO;2](http://journals.ametsoc.org/doi/10.1175/1520-0442(1993)006<0393:CDACTI>2.0.CO;2) doi:
1204 10.1175/1520-0442(1993)006<0393:CDACTI>2.0.CO;2
- 1205 Shell, K. M., Kiehl, J. T., & Shields, C. A. (2008, May). Using the Radiative Kernel
1206 Technique to Calculate Climate Feedbacks in NCAR’s Community Atmo-
1207 spheric Model. *Journal of Climate*, *21*(10), 2269–2282. Retrieved 2023-07-24,
1208 from <http://journals.ametsoc.org/doi/10.1175/2007JCLI2044.1> doi:
1209 10.1175/2007JCLI2044.1
- 1210 Sherwood, S. C., Bony, S., & Dufresne, J.-L. (2014, January). Spread in model cli-
1211 mate sensitivity traced to atmospheric convective mixing. *Nature*, *505*(7481),
1212 37–42. Retrieved 2023-02-22, from [http://www.nature.com/articles/](http://www.nature.com/articles/nature12829)
1213 [nature12829](http://www.nature.com/articles/nature12829) doi: 10.1038/nature12829
- 1214 Sherwood, S. C., Webb, M. J., Annan, J. D., Armour, K. C., Forster, P. M., Harg-
1215 reaves, J. C., ... Zelinka, M. D. (2020, December). An Assessment of Earth’s
1216 Climate Sensitivity Using Multiple Lines of Evidence. *Reviews of Geophysics*,
1217 *58*(4). Retrieved 2022-02-14, from [https://onlinelibrary.wiley.com/doi/](https://onlinelibrary.wiley.com/doi/10.1029/2019RG000678)
1218 [10.1029/2019RG000678](https://onlinelibrary.wiley.com/doi/10.1029/2019RG000678) doi: 10.1029/2019RG000678
- 1219 Siler, N., Roe, G. H., & Armour, K. C. (2018, September). Insights into the Zonal-
1220 Mean Response of the Hydrologic Cycle to Global Warming from a Diffusive
1221 Energy Balance Model. *Journal of Climate*, *31*(18), 7481–7493. Retrieved
1222 2023-03-07, from [https://journals.ametsoc.org/view/journals/clim/31/](https://journals.ametsoc.org/view/journals/clim/31/18/jcli-d-18-0081.1.xml)
1223 [18/jcli-d-18-0081.1.xml](https://journals.ametsoc.org/view/journals/clim/31/18/jcli-d-18-0081.1.xml) doi: 10.1175/JCLI-D-18-0081.1
- 1224 Slingo, J. M. (1980, October). A cloud parametrization scheme derived from
1225 GATE data for use with a numerical model. *Quarterly Journal of the Royal*

- 1226 *Meteorological Society*, 106(450), 747–770. Retrieved 2023-07-25, from
 1227 <https://onlinelibrary.wiley.com/doi/10.1002/qj.49710645008> doi:
 1228 10.1002/qj.49710645008
- 1229 Soden, B. J., Held, I. M., Colman, R., Shell, K. M., Kiehl, J. T., & Shields,
 1230 C. A. (2008, July). Quantifying Climate Feedbacks Using Radiative Ker-
 1231 nels. *Journal of Climate*, 21(14), 3504–3520. Retrieved 2022-05-26, from
 1232 <http://journals.ametsoc.org/doi/10.1175/2007JCLI2110.1> doi:
 1233 10.1175/2007JCLI2110.1
- 1234 Sourdeval, O., C.-Labonnote, L., Baran, A. J., Mülmenstädt, J., & Brogniez, G.
 1235 (2016, October). A methodology for simultaneous retrieval of ice and liq-
 1236 uid water cloud properties. Part 2: Near-global retrievals and evaluation
 1237 against A-Train products. *Quarterly Journal of the Royal Meteorolog-
 1238 ical Society*, 142(701), 3063–3081. Retrieved 2022-04-03, from [https://
 1239 onlinelibrary.wiley.com/doi/10.1002/qj.2889](https://onlinelibrary.wiley.com/doi/10.1002/qj.2889) doi: 10.1002/qj.2889
- 1240 Stephens, G. L. (1978, November). Radiation Profiles in Extended Water Clouds.
 1241 II: Parameterization Schemes. *Journal of the Atmospheric Sciences*, 35(11),
 1242 2123–2132. Retrieved 2023-08-24, from [http://journals.ametsoc.org/
 1243 doi/10.1175/1520-0469\(1978\)035<2123:RPIEWC>2.0.CO;2](http://journals.ametsoc.org/doi/10.1175/1520-0469(1978)035<2123:RPIEWC>2.0.CO;2) doi:
 1244 10.1175/1520-0469(1978)035<2123:RPIEWC>2.0.CO;2
- 1245 Stephens, G. L., & Ellis, T. D. (2008, December). Controls of Global-Mean Precip-
 1246 itation Increases in Global Warming GCM Experiments. *Journal of Climate*,
 1247 21(23), 6141–6155. Retrieved 2023-03-16, from [http://journals.ametsoc
 1248 .org/doi/10.1175/2008JCLI2144.1](http://journals.ametsoc.org/doi/10.1175/2008JCLI2144.1) doi: 10.1175/2008JCLI2144.1
- 1249 Stevens, B., & Brenguier, J.-L. (2009). *Cloud-controlling Factors*.
- 1250 Storelvmo, T., & Tan, I. (2015, July). The Wegener-Bergeron-Findeisen pro-
 1251 cess – Its discovery and vital importance for weather and climate. *Me-
 1252 teorologische Zeitschrift*, 24(4), 455–461. Retrieved 2023-01-18, from
 1253 [http://www.schweizerbart.de/papers/metz/detail/24/84731/The
 1254 _Wegener_Bergeron_Findeisen_process_Its_discov?af=crossref](http://www.schweizerbart.de/papers/metz/detail/24/84731/The_Wegener_Bergeron_Findeisen_process_Its_discov?af=crossref) doi:
 1255 10.1127/metz/2015/0626
- 1256 Storelvmo, T., Tan, I., & Korolev, A. V. (2015, December). Cloud Phase Changes
 1257 Induced by CO2 Warming—a Powerful yet Poorly Constrained Cloud-Climate
 1258 Feedback. *Current Climate Change Reports*, 1(4), 288–296. Retrieved 2023-
 1259 02-22, from <http://link.springer.com/10.1007/s40641-015-0026-2> doi:
 1260 10.1007/s40641-015-0026-2
- 1261 Tan, I., Oreopoulos, L., & Cho, N. (2019, April). The Role of Thermodynamic
 1262 Phase Shifts in Cloud Optical Depth Variations With Temperature. *Geo-
 1263 physical Research Letters*, 46(8), 4502–4511. Retrieved 2023-04-10, from
 1264 <https://onlinelibrary.wiley.com/doi/10.1029/2018GL081590> doi:
 1265 10.1029/2018GL081590
- 1266 Tan, I., Storelvmo, T., & Zelinka, M. D. (2016, April). Observational constraints on
 1267 mixed-phase clouds imply higher climate sensitivity. *Science*, 352(6282), 224–
 1268 227. Retrieved 2023-01-18, from [https://www.science.org/doi/10.1126/
 1269 science.aad5300](https://www.science.org/doi/10.1126/science.aad5300) doi: 10.1126/science.aad5300
- 1270 Terai, C. R., Klein, S. A., & Zelinka, M. D. (2016, August). Constraining the
 1271 low-cloud optical depth feedback at middle and high latitudes using satellite
 1272 observations: CONSTRAINING LOW-CLOUD OPTICAL DEPTH FEED-
 1273 BACK. *Journal of Geophysical Research: Atmospheres*, 121(16), 9696–9716.
 1274 Retrieved 2022-08-12, from <http://doi.wiley.com/10.1002/2016JD025233>
 1275 doi: 10.1002/2016JD025233
- 1276 Terai, C. R., Zhang, Y., Klein, S. A., Zelinka, M. D., Chiu, J. C., & Min, Q. (2019,
 1277 February). Mechanisms Behind the Extratropical Stratiform Low-Cloud Op-
 1278 tical Depth Response to Temperature in ARM Site Observations. *Journal of
 1279 Geophysical Research: Atmospheres*, 124(4), 2127–2147. Retrieved 2022-05-23,
 1280 from <https://onlinelibrary.wiley.com/doi/10.1029/2018JD029359> doi:

- 10.1029/2018JD029359
- 1281
1282 Trenberth, K. (2011, March). Changes in precipitation with climate change. *Cli-*
1283 *mate Research*, 47(1), 123–138. Retrieved 2023-03-16, from [http://www.int-](http://www.int-res.com/abstracts/cr/v47/n1-2/p123-138/)
1284 [res.com/abstracts/cr/v47/n1-2/p123-138/](http://www.int-res.com/abstracts/cr/v47/n1-2/p123-138/) doi: 10.3354/cr00953
- 1285 Tukey, J. W. (1958, June). Bias and Confidence in Not-quite Large Samples.
1286 (Abstracts of Papers). *The Annals of Mathematical Statistics*, 29(2), 614.
1287 Retrieved 2023-04-06, from [http://projecteuclid.org/euclid.aoms/](http://projecteuclid.org/euclid.aoms/1177706647)
1288 [1177706647](http://projecteuclid.org/euclid.aoms/1177706647) doi: 10.1214/aoms/1177706647
- 1289 Wall, C. J., Norris, J. R., Possner, A., McCoy, D. T., McCoy, I. L., & Lutsko, N. J.
1290 (2022, November). Assessing effective radiative forcing from aerosol–cloud
1291 interactions over the global ocean. *Proceedings of the National Academy of Sci-*
1292 *ences*, 119(46), e2210481119. Retrieved 2023-01-26, from [https://pnas.org/](https://pnas.org/doi/10.1073/pnas.2210481119)
1293 [doi/10.1073/pnas.2210481119](https://pnas.org/doi/10.1073/pnas.2210481119) doi: 10.1073/pnas.2210481119
- 1294 Webb, M. J., Lock, A. P., Bretherton, C. S., Bony, S., Cole, J. N. S., Idelkadi, A.,
1295 ... Zhao, M. (2015, November). The impact of parametrized convection on
1296 cloud feedback. *Philosophical Transactions of the Royal Society A: Mathe-*
1297 *matical, Physical and Engineering Sciences*, 373(2054), 20140414. Retrieved
1298 2023-02-22, from [https://royalsocietypublishing.org/doi/10.1098/](https://royalsocietypublishing.org/doi/10.1098/rsta.2014.0414)
1299 [rsta.2014.0414](https://royalsocietypublishing.org/doi/10.1098/rsta.2014.0414) doi: 10.1098/rsta.2014.0414
- 1300 Yettella, V., & Kay, J. E. (2017, September). How will precipitation change in extra-
1301 tropical cyclones as the planet warms? Insights from a large initial condition
1302 climate model ensemble. *Climate Dynamics*, 49(5-6), 1765–1781. Retrieved
1303 2023-02-05, from <http://link.springer.com/10.1007/s00382-016-3410-2>
1304 doi: 10.1007/s00382-016-3410-2
- 1305 Zelinka, M. D., Grise, K. M., Klein, S. A., Zhou, C., DeAngelis, A. M., & Chris-
1306 tensen, M. W. (2018, October). Drivers of the Low-Cloud Response
1307 to Poleward Jet Shifts in the North Pacific in Observations and Mod-
1308 els. *Journal of Climate*, 31(19), 7925–7947. Retrieved 2023-04-13, from
1309 <https://journals.ametsoc.org/doi/10.1175/JCLI-D-18-0114.1> doi:
1310 [10.1175/JCLI-D-18-0114.1](https://journals.ametsoc.org/doi/10.1175/JCLI-D-18-0114.1)
- 1311 Zelinka, M. D., Klein, S. A., & Hartmann, D. L. (2012, June). Comput-
1312 ing and Partitioning Cloud Feedbacks Using Cloud Property Histograms.
1313 Part II: Attribution to Changes in Cloud Amount, Altitude, and Optical
1314 Depth. *Journal of Climate*, 25(11), 3736–3754. Retrieved 2022-05-26, from
1315 <https://journals.ametsoc.org/doi/10.1175/JCLI-D-11-00249.1> doi:
1316 [10.1175/JCLI-D-11-00249.1](https://journals.ametsoc.org/doi/10.1175/JCLI-D-11-00249.1)
- 1317 Zelinka, M. D., Myers, T. A., McCoy, D. T., Po-Chedley, S., Caldwell, P. M., Ceppi,
1318 P., ... Taylor, K. E. (2020). *Causes of higher climate sensitivity in cmip6*
1319 *models* (Vol. 47) (software No. 1). Wiley Online Library.
- 1320 Zelinka, M. D., Myers, T. A., McCoy, D. T., Po-Chedley, S., Caldwell, P. M., Ceppi,
1321 P., ... Taylor, K. E. (2020, January). Causes of Higher Climate Sensitivity in
1322 CMIP6 Models. *Geophysical Research Letters*, 47(1). Retrieved 2021-11-29,
1323 from <https://onlinelibrary.wiley.com/doi/abs/10.1029/2019GL085782>
1324 doi: 10.1029/2019GL085782
- 1325 Zhai, C., Jiang, J. H., & Su, H. (2015, October). Long-term cloud change im-
1326 printed in seasonal cloud variation: More evidence of high climate sensitivity:
1327 Cloud Feedback and Seasonal Variation. *Geophysical Research Letters*, 42(20),
1328 8729–8737. Retrieved 2022-03-27, from [http://doi.wiley.com/10.1002/](http://doi.wiley.com/10.1002/2015GL065911)
1329 [2015GL065911](http://doi.wiley.com/10.1002/2015GL065911) doi: 10.1002/2015GL065911
- 1330 Zhang, Y., Xie, S., Lin, W., Klein, S. A., Zelinka, M., Ma, P., ... Ma, H. (2019,
1331 May). Evaluation of Clouds in Version 1 of the E3SM Atmosphere Model With
1332 Satellite Simulators. *Journal of Advances in Modeling Earth Systems*, 11(5),
1333 1253–1268. Retrieved 2023-08-23, from [https://onlinelibrary.wiley.com/](https://onlinelibrary.wiley.com/doi/10.1029/2018MS001562)
1334 [doi/10.1029/2018MS001562](https://onlinelibrary.wiley.com/doi/10.1029/2018MS001562) doi: 10.1029/2018MS001562
- 1335 Zhao, M. (2014, March). An Investigation of the Connections among Con-

1336 vection, Clouds, and Climate Sensitivity in a Global Climate Model.
1337 *Journal of Climate*, 27(5), 1845–1862. Retrieved 2023-02-22, from
1338 <http://journals.ametsoc.org/doi/10.1175/JCLI-D-13-00145.1> doi:
1339 10.1175/JCLI-D-13-00145.1
1340 Zheng, Y., Rosenfeld, D., & Li, Z. (2020, July). A More General Paradigm for
1341 Understanding the Decoupling of Stratocumulus-Topped Boundary Lay-
1342 ers: The Importance of Horizontal Temperature Advection. *Geophys-
1343 ical Research Letters*, 47(14), e2020GL087697. Retrieved 2023-08-24, from
1344 <https://agupubs.onlinelibrary.wiley.com/doi/10.1029/2020GL087697>
1345 doi: 10.1029/2020GL087697

Figure 1.

Relationships between SW_{FB} , LWP Response $\left(\frac{\Delta LWP}{\Delta GMT}\right)$, and Climate Sensitivity

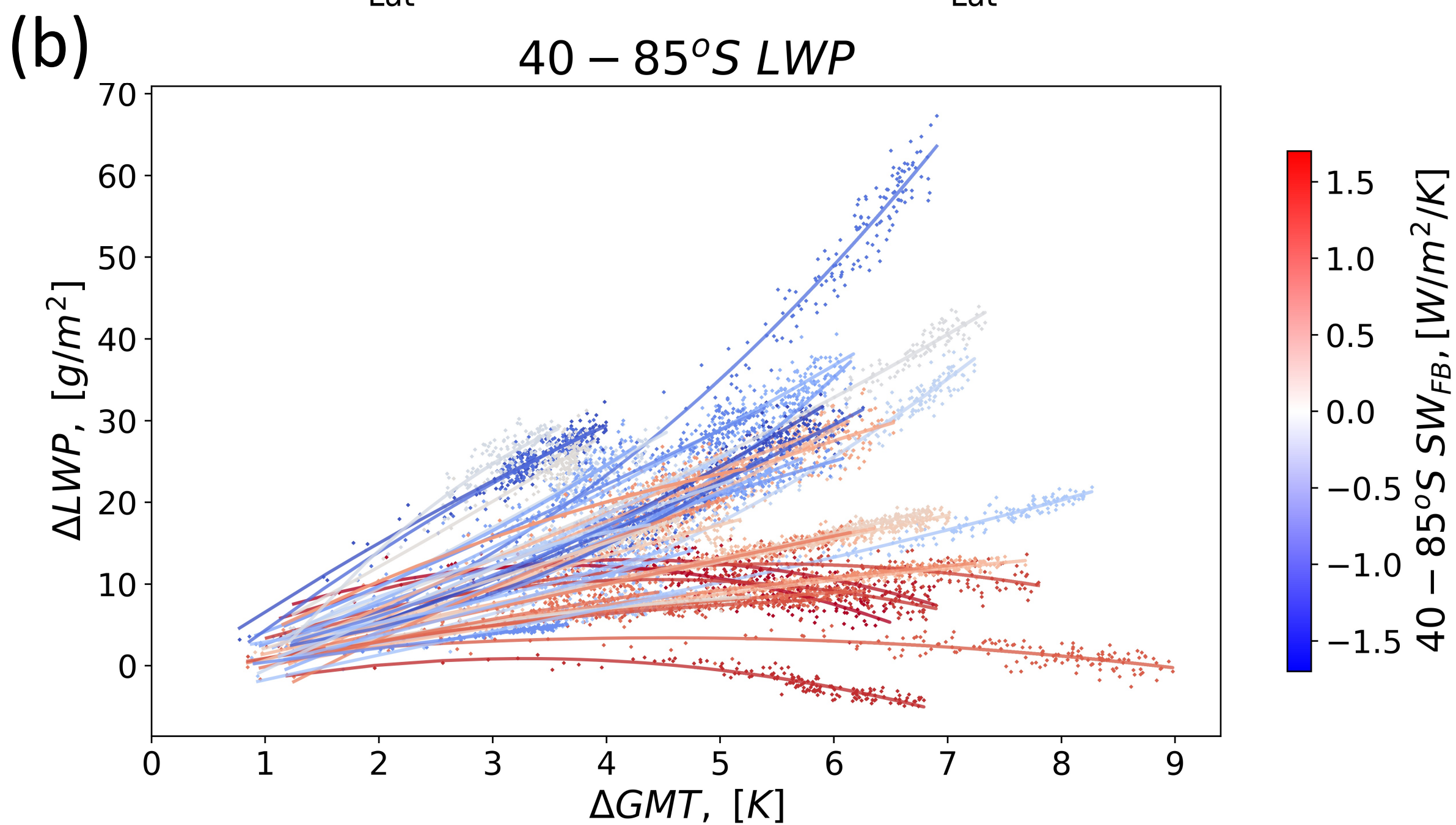
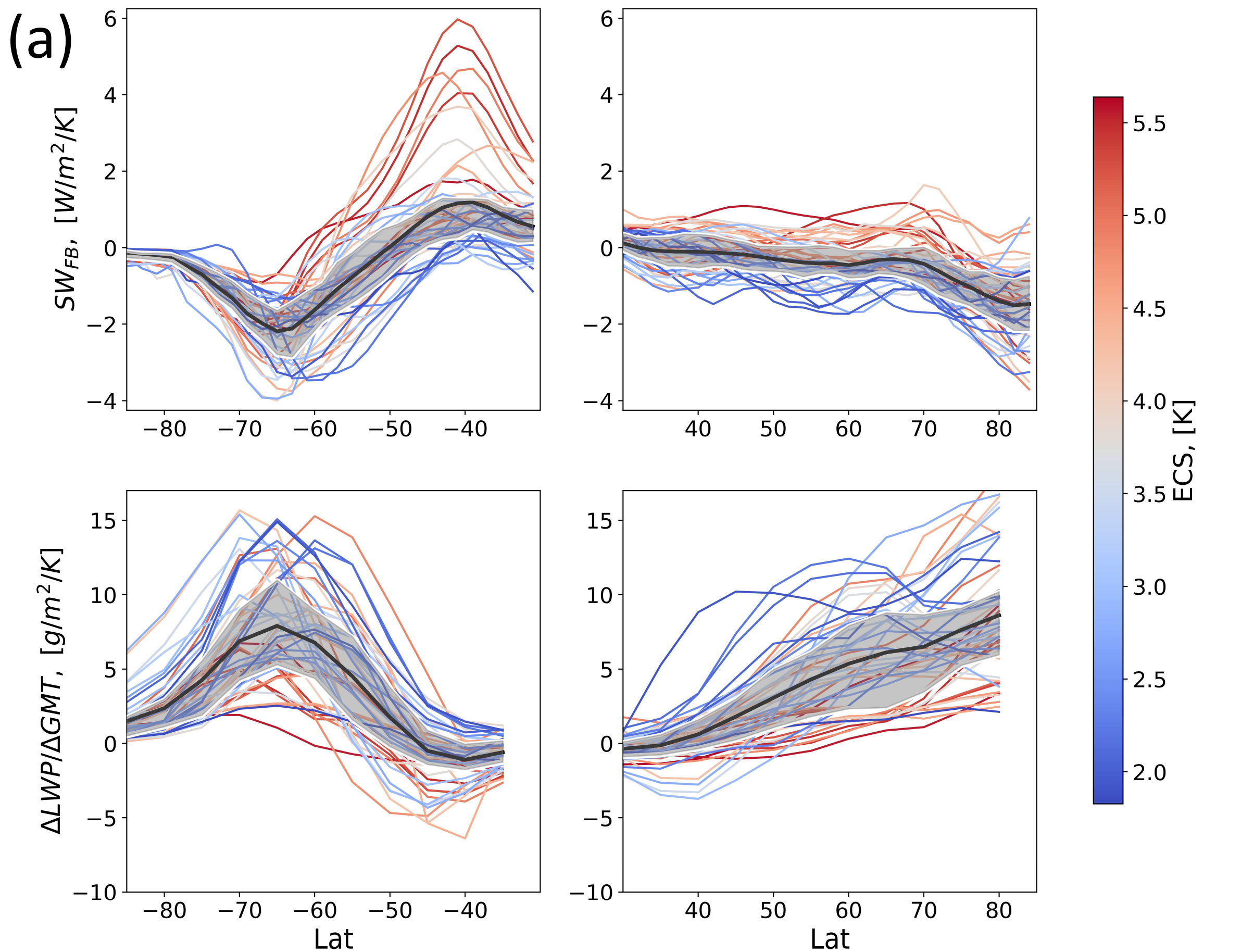
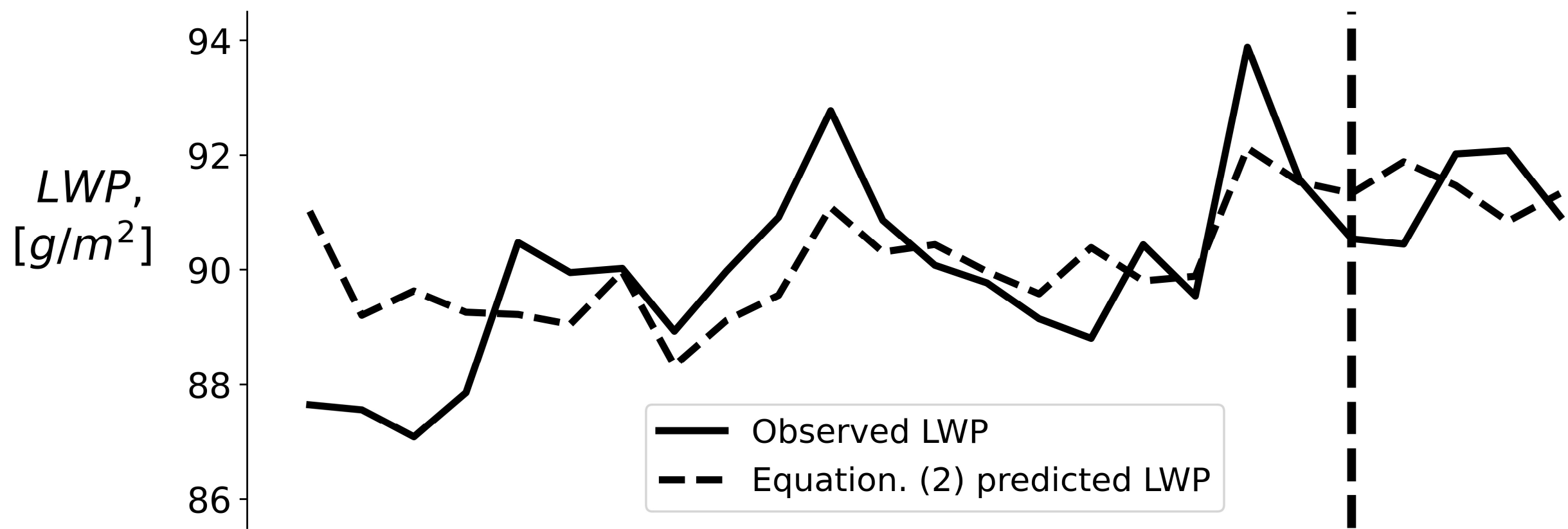


Figure 2.

Prediction of Observed LWP

(a) 1992 - 2016 Southern Ocean LWP



(b) CCF Contributions to LWP Response

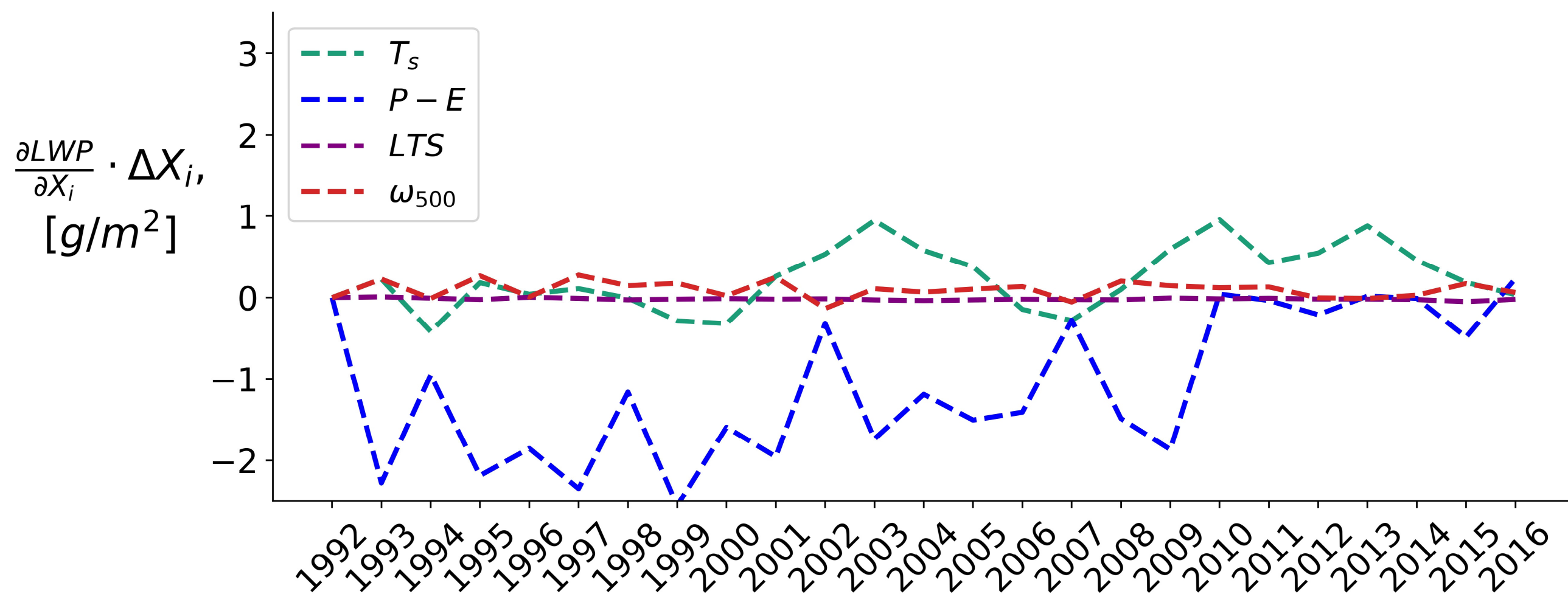


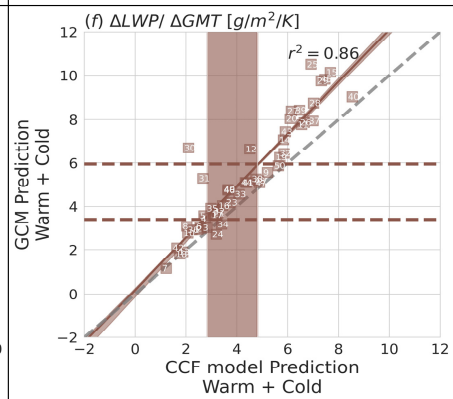
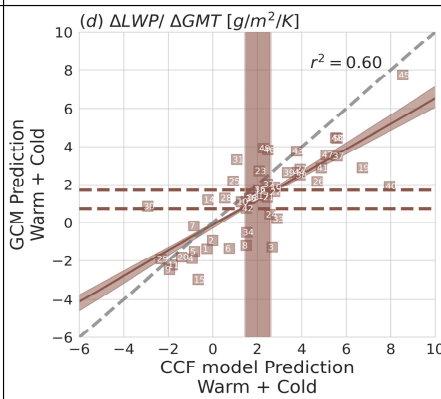
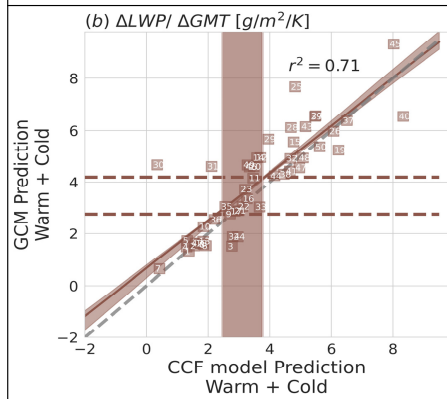
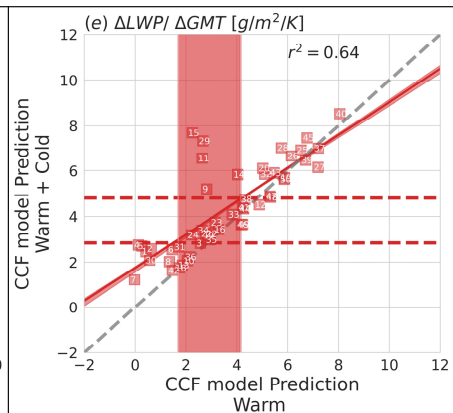
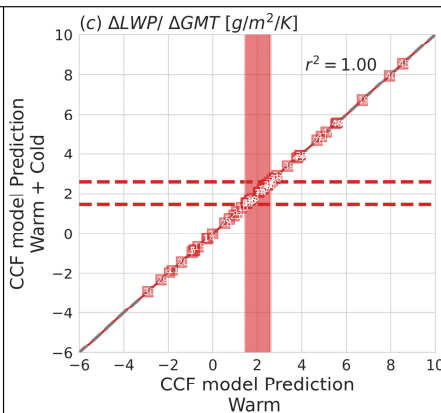
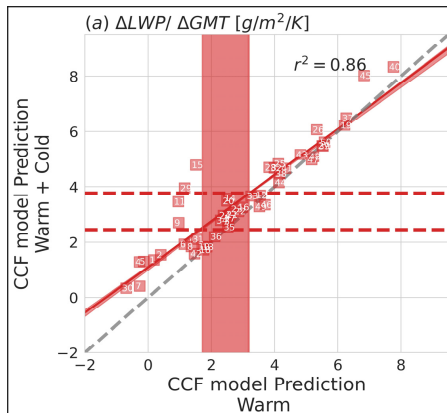
Figure 3.

Constraints on GCM LWP Response ($\frac{\Delta LWP}{\Delta GMT}$)

40 – 85° S

40 – 50° S

50 – 85° S



CCF (Warm)
→ CCF (Both)

CCF (Both)
→ GCM (Both)

Figure 4.

Decomposition on LWP Response ($\frac{\Delta LWP}{\Delta GMT}$)

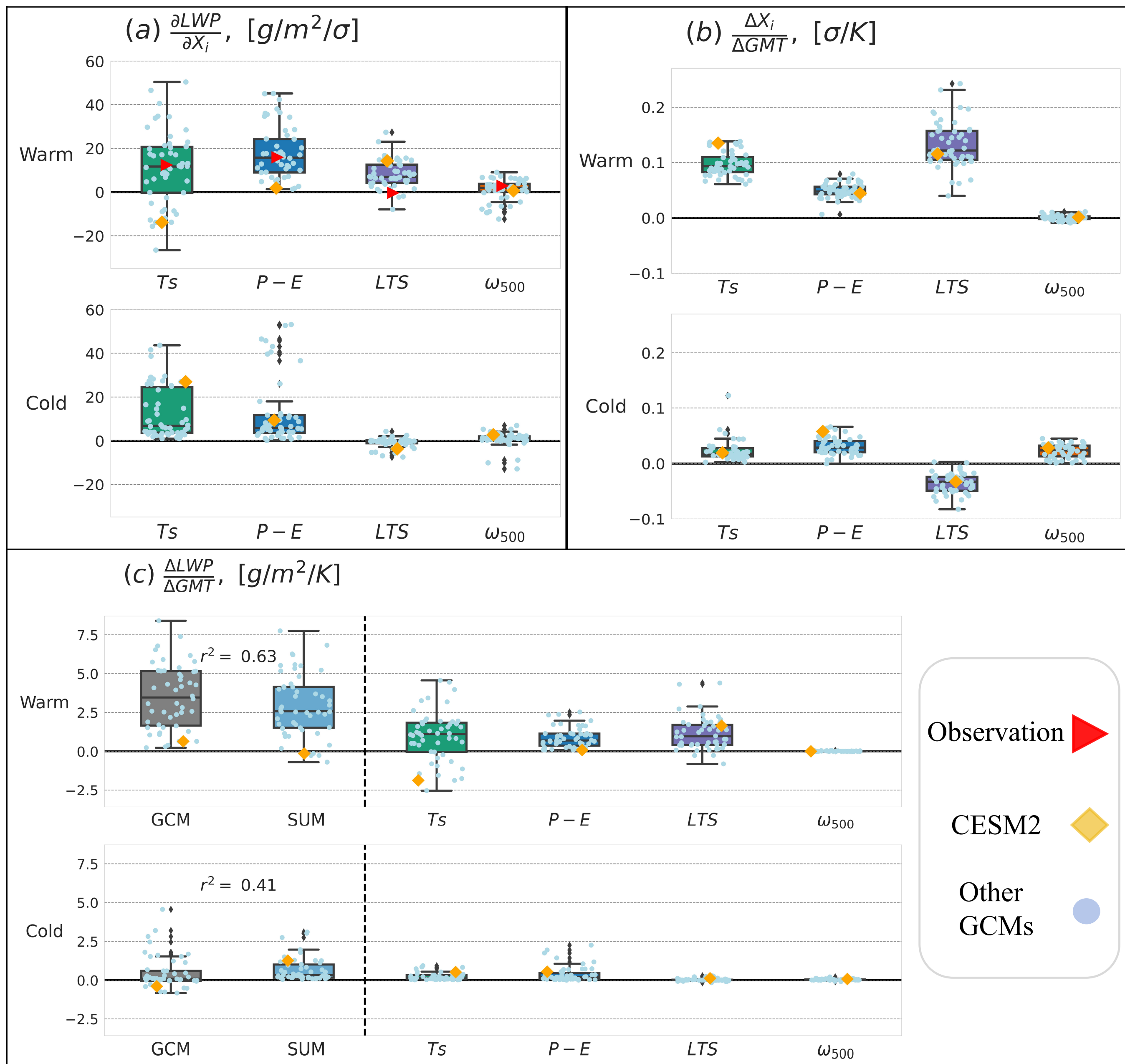


Figure 5.

Constraint on Radiative Susceptibility ($\frac{\partial \alpha}{\partial LWP}$)

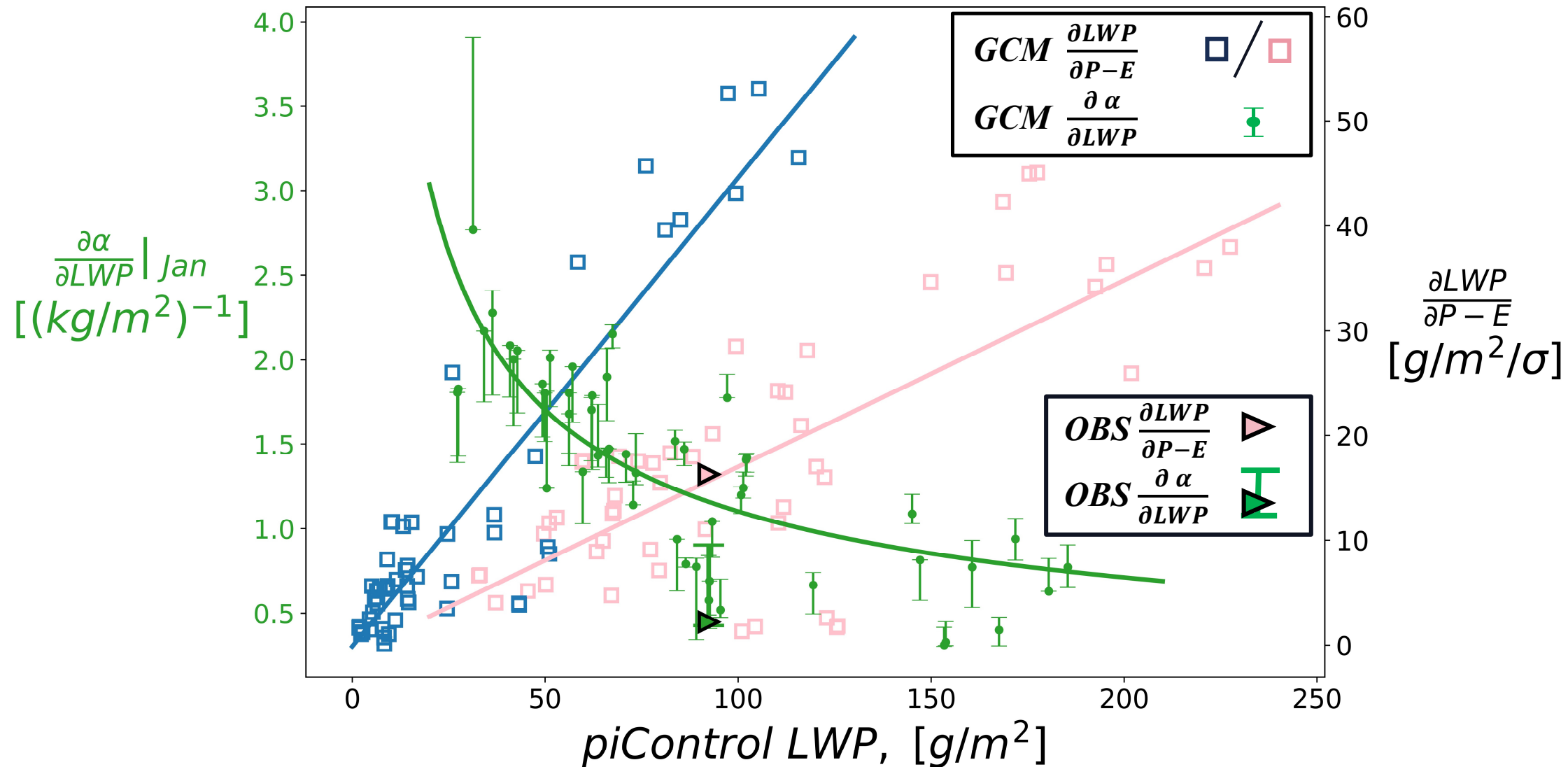


Figure 6.

Constraint on Shortwave Cloud Feedback (SW_{FB})

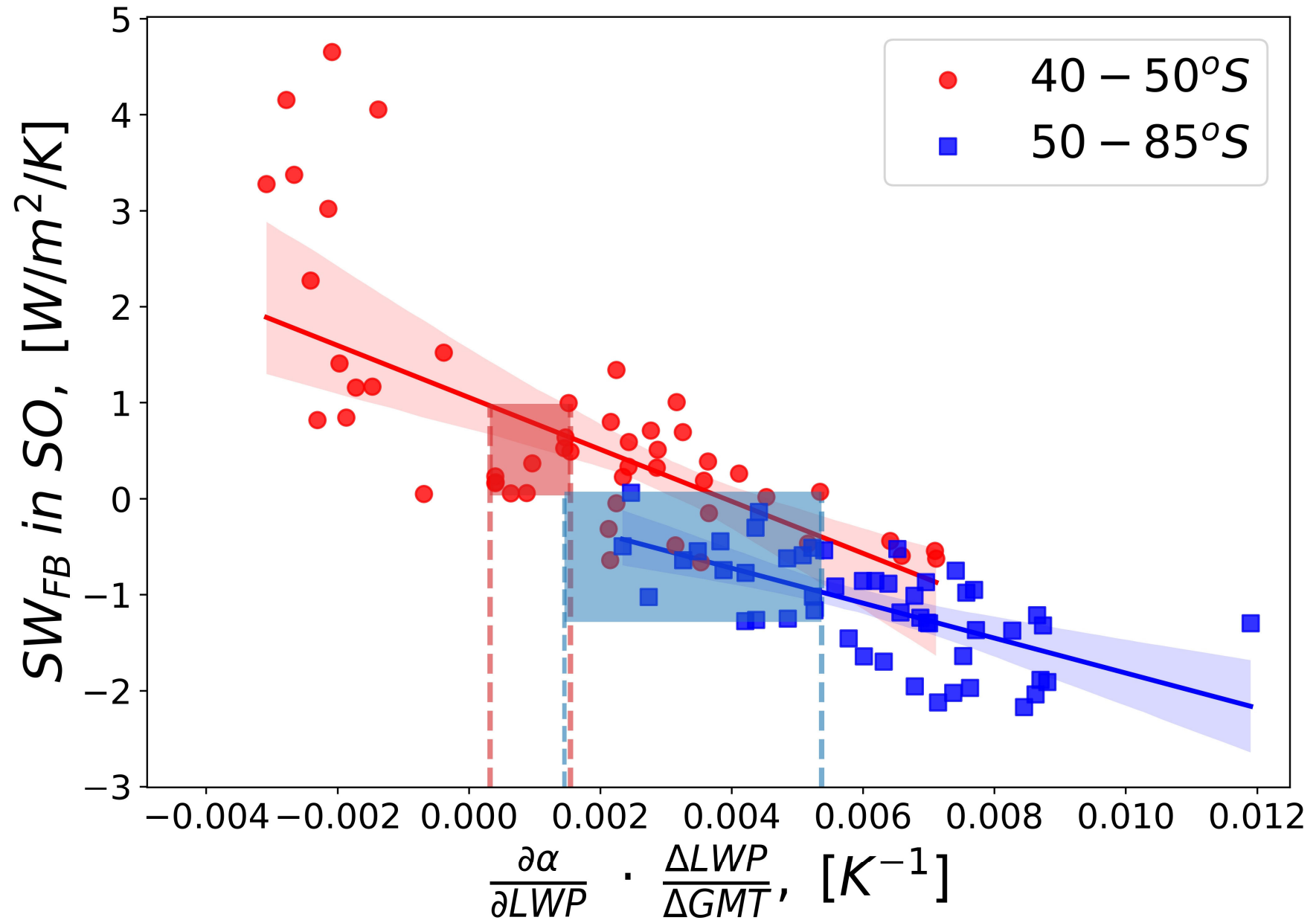


Figure 7.

Number of GCMs

